JAERI-M
84-195

PLASMA BEHAVIOR AND PLASMA-WALL INTERACTION IN MAGNETIC FUSION DEVICES

October 1984

Hideo OHTSUKA

日本原子力研究所
Japan Atomic Energy Research Institute

JAERI-Mレポートは，日本原子力研究所が不定期に公刊している研究報告書です。
入手の問合わせは，日本原子力研究所技術情報部情報資料課（〒319-11茨城県那珂郡東海村）あて，お申しこしください。なお，このほかに財団法人原子力弘済会資料センター（〒319-11 茨城県那珂郡東海村日本原子力研究所内）で複写による実費頒布をおこなっております。

JAERI-M reports are issued irregularly.
Inquiries about availability of the reports should be addressed to Information Section, Division of Technical Information, Japan Atomic Energy Research Institute, Tokai-mura, Naka-gun, Ibaraki-ken 319-11, Japan.

©Japan Atomic Energy Research Institute, 1984

編集兼発行　日本原子力研究所
印　　刷　いばらき印刷㈱

JAERI-M 84-195

Plasma Behavior and Plasma-Wall Interaction in Magnetic Fusion Devices

Hideo OHTSUKA

Department of Thermonuclear Fusion Research,
Tokai Research Establishment, JAERI

(Received October 4, 1984)

To study the fundamental behavior of plasma in magnetic field is the main subject in the early stage of the magnetic fusion research. At the next stage, it is necessary to overcome some actual problems in order to attain reactor grade plasmas. One of them is to control impurities in the plasma. In these points of view, we carried out several experiments or theoretical analyses. Firstly, anomalous loss mechanisms in magnetic field were investigated in a toroidal multipole device JFT-1 and the role of motions of charged particles in the magnetic field was exhibited. Various measurements of plasma in the scrape-off layer were made in a divertor tokamak JFT-2a and in an ordinary tokamak JFT-2. The former study demonstrated the first successful divertor operation of the tokamak device and the latter one clarified the mechanism of arcing on the tokamak first wall. As to arcing, a new theory which describes the retrograde motion, the well known strange motion of arcs in a magnetic field, was proposed. Good agreement with the experimental results was shown. Finally, by considering a zero-dimensional sputtering model a self-consistent relation between light and metal impurities in tokamak plasmas was obtained. It was shown that the relation well describes some fundamental aspects of the plasma-wall interaction. As a conclusion, the importance of simple behavior of charged particles in magnetic fields was pointed out not only for the plasma confinement but also for the plasma-wall interaction.

Keywords; Confinement, Anomalous Plasma Loss, Convection Cell, Multipole Device, Divertor Tokamak, Scrape-off Layer, Electrostatic Probe, Divertor Efficiency, Plasma Flow, Diffusion Coefficient, Unipolar Arcing, Retrograde Motion, Zero-dimensional Impurity Model

JAERI－M 84－195

磁気核融合装置におけるプラズマの挙動とプラズマ壁相互作用

日本原子力研究所東海研究所核融合研究部
大塚英男

（1984年10月4日受理）

磁気閉じ込め方式による熱核融合の研究開発における最初の課題は，磁場中のプラズマの基本的な挙動を調べることであろう。次の炉心プラズマ達成までの過程では実際的な問題への対応が必要となる。その1つとして，プラズマ中の不純物の制御という課題がある。本報告では，これらを課題として行われた実験的，理論的な研究結果を述べる。はじめに，環状マルチポール装置であるJFT－1を用いて磁場中の荷電粒子のふるまいとそれに関係したプラズマの損失機構について調べる。つぎに，ダイバータ付トカマク装置であるJFT－2aにおいては周辺部プラズマの測定にもとづいてダイバータの機能などを調べる。つづいて標準的トカマク装置であるJFT－2をもちいて，不純物混入過程の1つの第一壁面でのアークについて調べる。周辺プラズマの測定と対応させて，アーク発生の機構及びその制御の方法を明らかにする。ここで同時に，このアークが示す特異な現象である逆行現象についての考察を行い，観測事実と良い一致を示す理論を提出する。最後に，トカマク中の不純物を軽元素不純物と金属不純物に分けて全体的に見た時に，後者が前者の関数で表わすこののできる1つのモデルを提案する。それが実験結果と一致すること，そして不純物の挙動の理解に有効であることを示す。結論として磁場中のプラズマの挙動とプラズマ壁相互作用との密接な関連を指摘する。

Contents

目　　次

I INTRODUCTION

At the opening adress of the first International Conference on Peaceful Uses of Atomic Energy (Geneva, 1955), Dr. H. Bhabha President of the conference said "I venture to predict that a method will be found for liberating fusion energy in a controlled manner within the next two decades. When that happens, the energy problems of the world will truly have been solved forever for the fuel will be as plentiful as the heavy hydrogen in the oceans" [1]. It is about that time after which the controlled thermonuclear fusion research in the early stage has gradually opened in the literature. The difficulties in both physical and technological problems which would be encountered through the research were well understood from the beginning. International co-operation of the research has therefore been organized by International Atomic Energy Agency. Intensive studies have begun mainly on magnetically confined plasmas. Against Dr. Bhabha's prospect, the progress in the subsequent researches seemed to be rather slow. His prospect was optimistic.

It was tokamak experiments of the 1970's, however, that threw the light on the fusion research. The fact that the tokamak leads the confinement race is considered to owe to its characteristics: for example, small β value and the simple magnetic field configuration where β represents a ratio of plasma pressure to that of the magnetic field. Furthermore, the favorable results of the tokamak can be understood from another point of view: plasma-wall interaction. For example, almost all pinch experiments

have encountered a limitation given by impurity radiation which cools the plasma. Impurities seem to be swept from the wall into the plasma by the plasma itself during the pinch phase. At the initial phase of tokamak discharges, impurities may be introduced into the plasma in the similar way to the pinch. However, since the plasma duration of the tokamak is much longer than the impurity confinement time, the initially introduced impurities do not affect the plasma after the lapse of the confinement time. That may be the reason why the tokamak overcomes the radiation barrier which limitted the pinch results. As a matter of course, the end-loss problem peculiar to open-end devices is another, and a direct, example. We may say that the plasma-wall interaction constitutes an important part of the confinement study. Actually, the promotion of the tokamak result owes largely to understanding of the plasma-wall interaction. For example, recent conditioning methods for the first-wall and also appropriate material selection have broaden the parameter range of the tokamak operation. Since we talk about the tokamak frequently through this thesis, let us here introduce it briefly. Figure 1 shows a schematic diagram of a typical tokamak. The confinement device is basically characterized by the magnetic field configuration. The most characteristic feature of the tokamak consists in the plasma current which is produced by magnetic induction by using, in general, a transformer core. The magnetic field by the plasma current is called poloidal field and plays an important role, viz. the plasma confinement. The plasma current is also used to heat the plasma itself; that is called Joule or Ohmic heating. The effeciency of Joule heating decreases with an increase of the

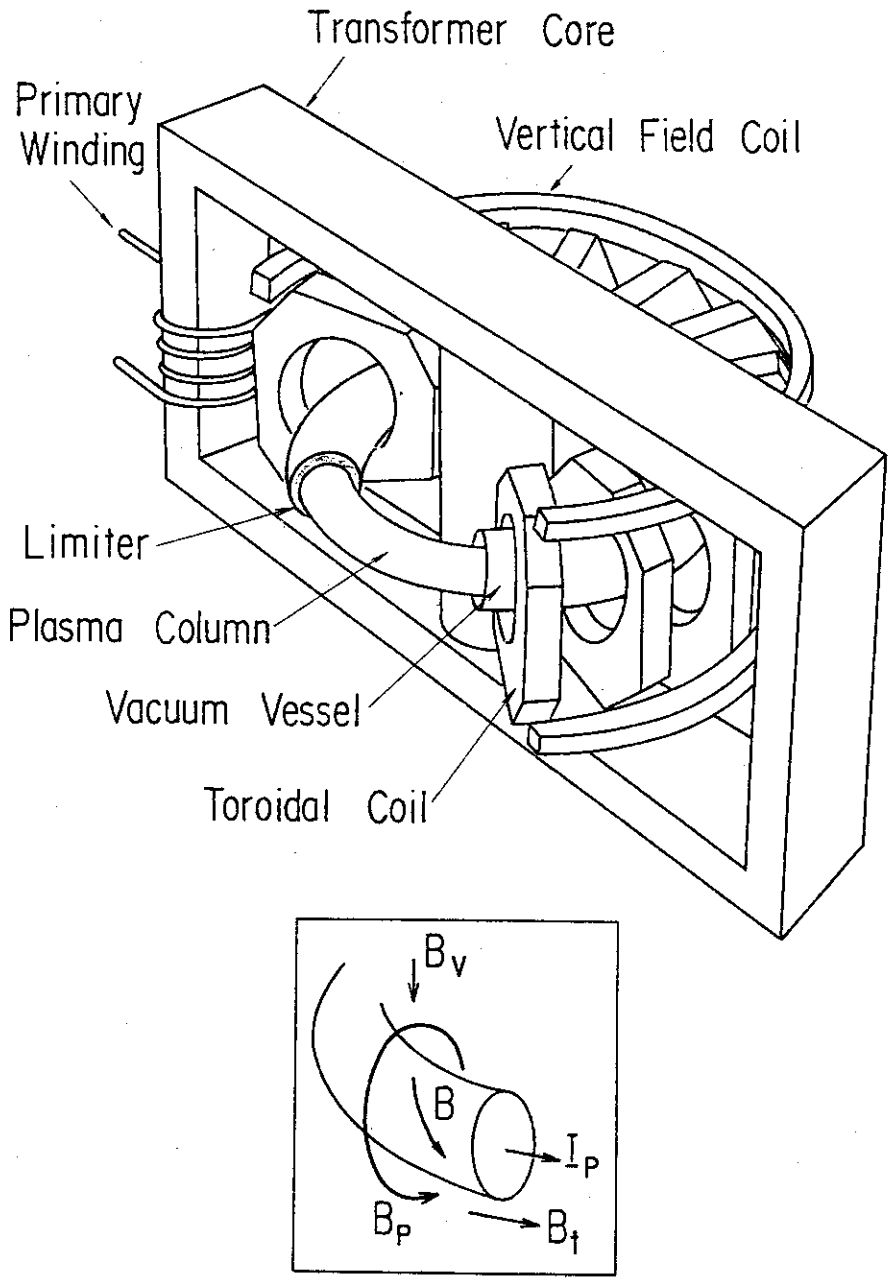

Fig. 1 Schematic diagram of a typical tokamak. Each component of the magnetic field (poloidal field B_p, toroidal field B_t, vertical field B_v) in the plasma column and resulting helical magnetic field B are illustrated in the inset where I_p designates the plasma current.

plasma temperature. Therefore, additional heating is necessary to atain a reactor grade plasma. The toroidal field which stabilizes plasma instabilities is made by the toroidal coil. The strong toroidal field as compared to the plasma pressure is one of the characteristics. Other basic magnetic field is the vertical field which stabilizes the plasma position. The tokamak magnetic field is, then, axisymmetric. This symple field configuration is also one of the characteristic aspects.

The plasma confined in the magnetic field inevitably contacts with the vessel wall because the plasma can not help flowing across the magnetic field owing to the diffusion process. Limiters are, in genral, provided at the inner vessel wall in order to protect wall materials against the plasma impact. The limiters are also used to determine the size of the plasma column. As the result, the limiters suffer intense plasma flux. Phenomena which are originated from the contact of the plasma with the vessel wall is called plasma-wall interaction. Therefore, the dominant plasma-wall interaction is considered to occur on the limiters. Usually, we call the vessel wall including the limiters the first-wall.

In this thesis, we study behavior of plasma in a magnetic field and the plasma-wall interaction in the tokamak. In the next chapter, we present an experimental result obtained with a toroidal multipole device with emphasis on plasma loss mechanisms. The experiment shows that simple motions of the charged particles in the magnetic field govern one of loss mechanisms. Conversly speaking, we exhibit plasma motions in a magnetic field which obey simple theories. This result is important for the magnetic fusion research. In Chap. 3, we examine a plasma in the

scrape-off-layer of a divertor tokamak. To know plasma parameters in the boundary region (scrape-off-layer) is important not only for the divertor experiments but also for understanding of the plasma-wall interaction of the ordinary tokamaks. We present here the first measurement of plasma in the scrape-off-layer of the divertor tokamak. Moreover, through these experiments, we exhibit the usefulness of electrostatic measurements. In Chap. 4, a study of unipolar arcing is presented. This phenomenon is caused by a contact of plasma with metalic wall. It causes impurity introduction into the plasma. Hence, this phenomenon is a typical plasma-wall interaction. The result of the study enables us to predict the future problem related to arcing in tokamaks. In the second part of the chapter, we analyze a motion of arcs in the magnetic field called retrograde motion. This peculiar phenomenon was first found at the beginning of this century and has not yet been given any reasonable explanation to its mechanism. We present a new theory which can sufficiently explain the known behavior. It is interesting to note that the theory is based upon a motion of a charged particle in magnetic field, which constitutes an important part of the frame-work of this thesis. In Chap. 5, we consider the gloval impurity problem in the tokamak plasma focussing our interest on a relation between light impurity and metal impurity. We make a simple model based on a fact that metal impurities in a plasma are mainly introduced by sputtering. It is shown that the model well describes gloval impurity behavior known in tokamak experiments and can be used as a model to understand basic impurity problems in the tokamak plasma. In Chap. 6, we summarize the

results obtained during the course of this study.

REFERENCE

[1] H. Bhabha, in Peaceful Uses of Atomic Energy (Proc. 1st Int. Conf. Geneva, 1955) Vol. 35, UN, New York (1956) p 35.

2 Particle Motion and Plasma Loss in a Toroidal Multipole.

§1. Introduction

The subject in early stage of controlled thermonuclear fusion research is to examine fundamental plasma behavior in magnetic fields: 1) to show whether the behavior agrees with the theoretically predicted one or not, 2) if not, to clarify the reason of the unexpected behavior.

In this chapter, we describe a study of a plasma confined in a toroidal multipole device (JFT-1). The toroidal multipole field can be established by setting several ring currents coaxially and by supplying appropriate amount of currents. Figure 1 shows the cross-section of JFT-1 together with its magnetic field configuration (hexapole field). The hatched circles in the figure show the conductors (hoop) and curved lines show resulting magnetic field lines and also surfaces of constant magnetic flux. The average magnetic field along a field line

$$\langle B \rangle = \int d\ell / \int \frac{1}{B} d\ell$$

becomes local minimum on ψ_s(separatrix) and local maximum on ψ_c (critical stability limit). The plasma is confined stably between the conductors and ψ_c. Because the plasma pressure is much smaller than the pressure of the magnetic field in multipole devices, a stable, quiet and reproducible plasma can be obtained

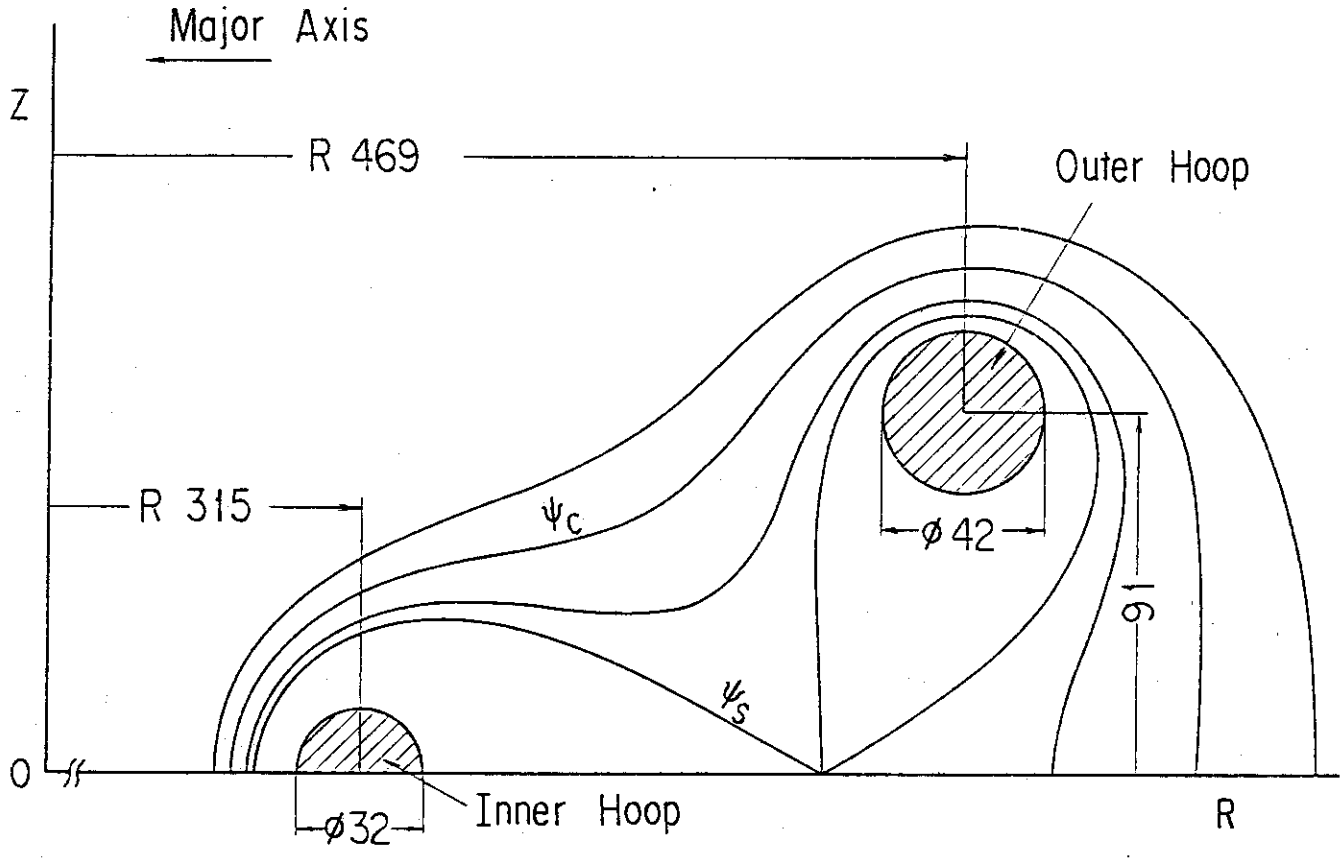

Fig. 1 Cross-section of JFT-1. Solid lines represent surfaces of constant magnetic flux and also field lines. The separatrix and the critical stability limit are indicated by ψ_s and ψ_c, respectively. This figure shows upper-half of the configuration which is symmetric with respect to the median plane (Z=0).

during experiments. The multipole devices are, thus, suitable for studies of fundamental plasma behavior in toroidal magnetic configuration.

The aim of the present study is to clarify one of anomalous loss mechanisms of plasma confined in a multipole device. We defined here anomalous loss as cross-field plasma losses without collisional diffusion. Collision is considered to govern the diffusion in a magnetic field with the relation $D = \nu\rho^2$ where D is the particle diffusion coefficient, ν is the collision frequency and ρ is the ion Larmor radius. If we obtain experimentally a diffusion coefficient whose value much exceeds an estimation from the above relation, we should say there exists anomalous loss mechanisms. So far, every multipole has exhibited anomalous confinement characteristics. Therefore, an important problem is to clarify the anomalous loss processes. Candidates of the cause of the anomalous loss now we consider of the multipole devices are error field, fluctuation and convection.

Error field is caused mainly due to misalignment of the coils. More or less, the actual coil set-up deviates from the ideal current positions. If an error field exists in the device, the plasma can escape easily from the confinement region along the stray field lines. Effectively, this loss is observed as if there exists an anomaly in the cross-field motion. Fluctuation in a plasma is caused by some instabilities. In general, the confined plasma has density and/or temperature gradient in the peripheral region, which is understood as a cause of the drift (universal) instabilities. The fluctuation in the plasma is considered to enhance the plasma loss because it produces small scale plasma

convection by the potential fluctuation or it enhances stochastic plasma motion when the state is turbulent. A rather large scale plasma flow is called convection. The cross-field convection is caused by an electric field in the plasma which is introduced by several mechanisms. Supports for the internal conductors are one of origins of the convection because they disturb the plasma and can produce an electric field perpendicular to the magnetic field.

In the following, we present results of a study on anomalous plasma loss in JFT-1 with emphasis on the support induced convection.

§2. Experiments

JFT-1 is a toroidal hexapole device aimed at studying the magnetically confined plasma. Details of the device have been described elsewhere [1]. The experimental conditions during the course of the study were as follows: the plasma was produced by electron cyclotron resonance of 2.45 GHz microwave with 3 kW power and 0.5 ms duration; average magnetic field on ψ_c was 1.33 kG; herium was employed as working gas. The currents for the hexapole field were supplied with a condenser bank. Hence, the wave form of the current was sinusoidal with quarter period of 8 ms. The microwave was applied at the flat top of the current and we used the after-glow plasma for the experiment. Typical plasma parameters are: electron temperature T_e = leV and electron density $n_e = 10^{10} - 10^{11}$ cm^{-3}. Although the cyclotron resonance of 2.45 GHz takes place at a magnetic field of 875 gauss, the

peak of the plasma density lies on the separatrix in the after-glow phase as seen lately in Fig. 7. The set-up of this experiment is shown in Fig. 2. In this figure, a part of the outer hoop is shown. On the surface of the hoop a model support of 10 mm diameter made of stainless steal was introduced in order to simulate the actual supports. The model support is removable for a comparison between cases with and without the support. Round the hoop, we wound insulated metal belts as hoop loss collectors and also set metal plates outside of ψ_c as wall loss collectros as shown A,B,C,D and L,M, respectivley, in the figure. These collectors can be electrically biased in order to repell electrons and collect ion flux only. The ion flux is considered as the plasma flux because the plasma motion is determined by ions which carry most of the plasma mass.

Here, we define a local co-ordinate X and Z near the model support as shown in Fig. 2 and also define the polarity of the poloidal magnetic field positive ($+B_p$) when the current flows in the direction indicated by the arrow in the figure. In order to measure plasma parameters, mainly floating potential ϕ_f, a Langmuir probe is used.

§3. Results

Figure 3 shows changes in hoop/wall loss fluxes as a result of the introduction of the model support with a dependence on the polarity of the magnetic field. Here, the ratio Γ_s/Γ_0 is shown where Γ_s and Γ_0 are ion fluxes with and without the model support, respectively. At the first glance, it can be seen that the intro-

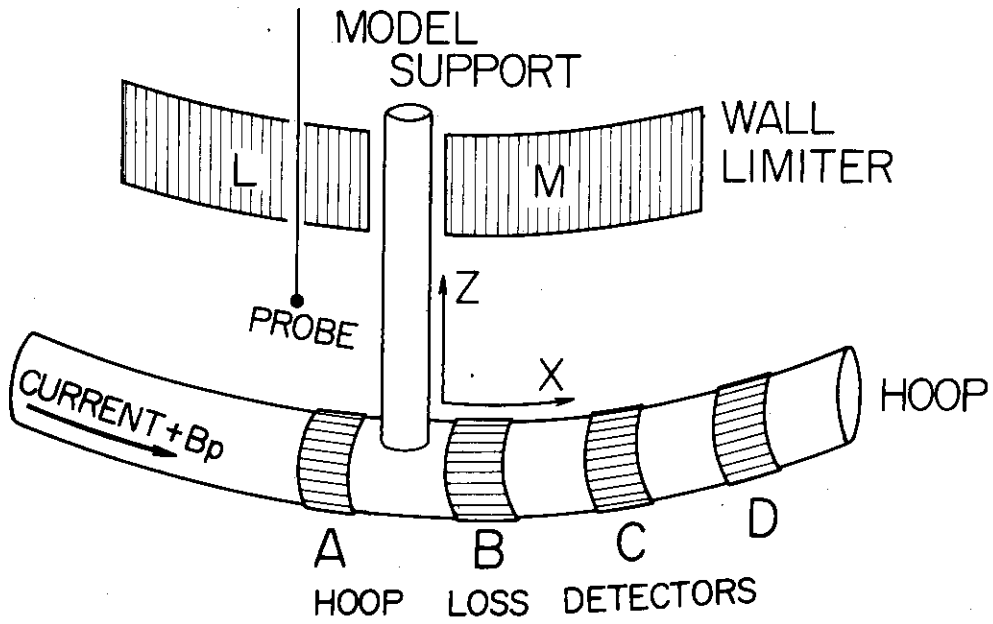

Fig. 2 Set-up for the experiment. The origin of the local co-ordinates (X,Z) is set at the contact point of the model support with the hoop.

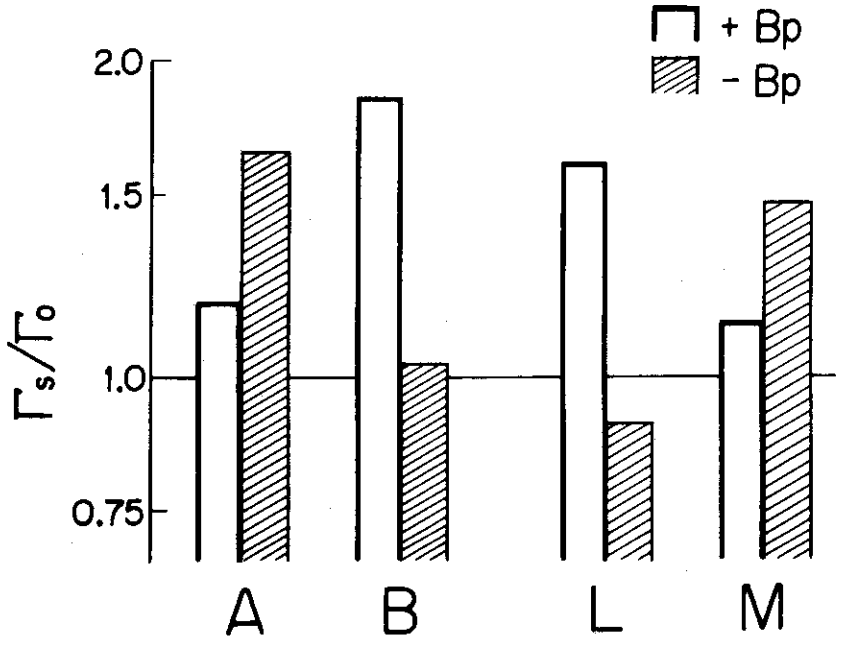

Fig. 3 Changes in hoop/wall loss fluxes as a result of the introduction of the model support where Γ_s and Γ_o are loss fluxes with and without the support, respectively.

duction of the model support resulted in an enhancement of loss fluxes. Second, the change in loss flux pattern with the change of polarity of B_p is just antisymmetric with respect to both the model support and the separatrix: the changes in loss flux to A and B are similar to that to M and L, respectively. The apparent dependence of the flux pattern on the polarity of B_p implies that the enhanced losses are due to some co-operative effect of the support and the magnetic field.

Figure 4 shows floating potential profiles in the X-direction where Fig. 4a and 4b were obtained inside and outside the separatrix, respectively. These profiles also exhibit antisymmetric behavior about the model support (X=0) and the separatrix when the polarity of B_p is changed.

The most probable mechanism which causes such a potential is the drift motion of charged particles in inhomogeneous magnetic field (grad B drift). In the figure, the direction of the grad B drift motion of ion is illustrated for each case. In general, particles have a compcnent of the motion parallel to the magnetic field. Hence, the actual drift orbit of a particle is a combination of the grad B drift and the circulating motion around the hoop. Let us consider, by using Fig. 4, a situation where an obstacle is introduced into the plasma under such motions. Ions moving in grad B drift direction are stopped by the obstacle (model support). In the right hand side of the support near the hoop, a lack of ions thus can be produced and vice versa for electrons. The resulting electric potential appears positive at the up-stream side and negative at the down-stream side of the support in the ion grad B drift direction. The potential profiles

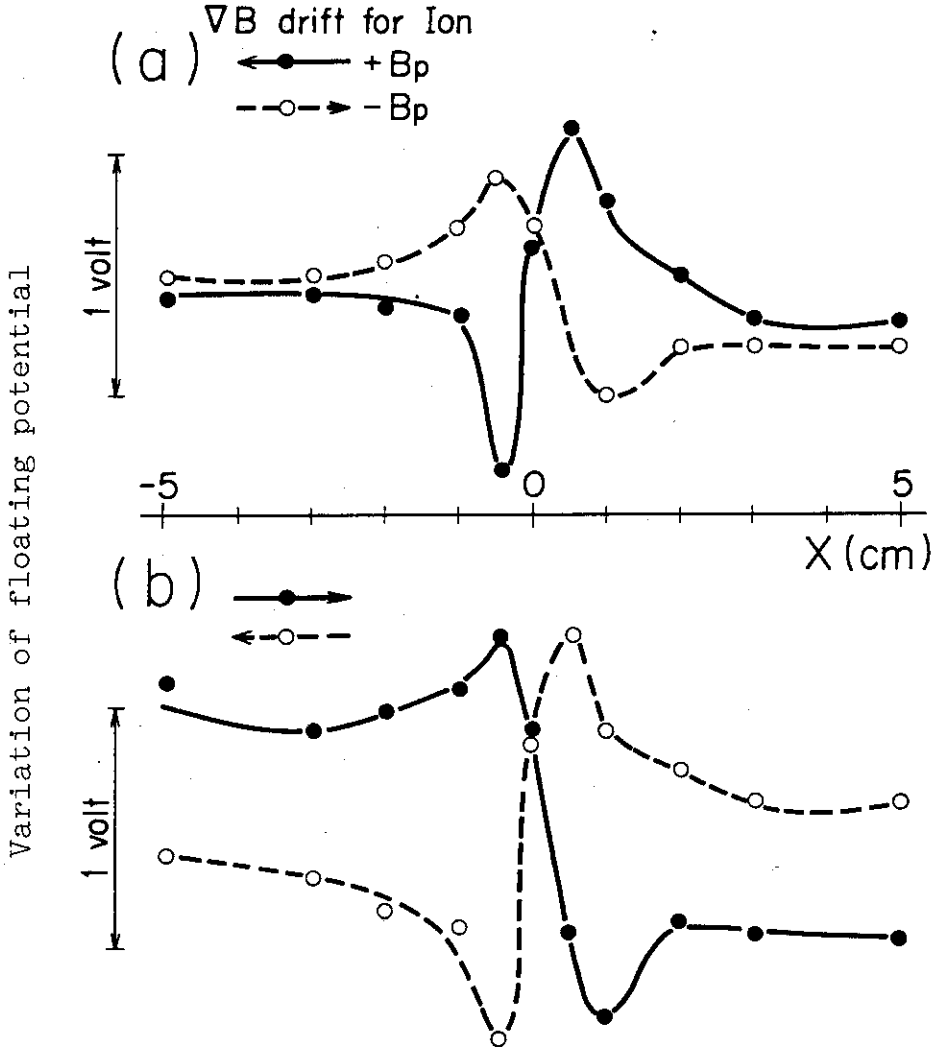

Fig. 4 Variations of floating potential across the model support ; a) outside the separatrix (Z=16 mm), b) inside the separatrix (Z=6 mm).

shown in Fig. 4 all agree with this explanation. Figure 5 shows a profile of the floating potential change $\Delta\phi_f$ along the support at X = -5 mm when the model support was introduced. The polarity of $\Delta\phi_f$ reversed just at the separatrix. This result also supports the mechanism mentioned above.

The spatial variation of the electric potential (namely, electric field) causes a flow of plasma in a magnetic field: so called ExB flow. Note that we consider here that the variation of the space potential is similar to that of the floating potential qualitatively. The electric fields in Fig. 4 cause the ExB flow in such a way that the plasma is removed from the confinement region. This tendency agrees with the overall enhancement of the loss fluxes shown in Fig. 3. However, it does not explain the asymmetric loss flux pattern seen in the figure. An additional azimuthal (X-direction) electric field is necessary near the model support. A careful measurement of the floating potential across the model support was carried out on the separatrix where no potential perturvation by the grad B drift exists. The result is shown in Fig. 6. On the separatrix, the potential appears less negative near the support independently on the polarity of B_p. This profile exhibits an additional azimuthal electric field near the support. The flux pattern of Fig. 3 agrees with the ExB flow produced by such an electric field. Figure 7 also supports the convection by a different point of view. This figure shows density profiles at X = -5 mm in the Z-direction. A shift of the profile by a change of the polarity of B_p can be found in this figure. The direction of the shift is consistent with the ExB convection mentioned here. Such a potential is caused by an

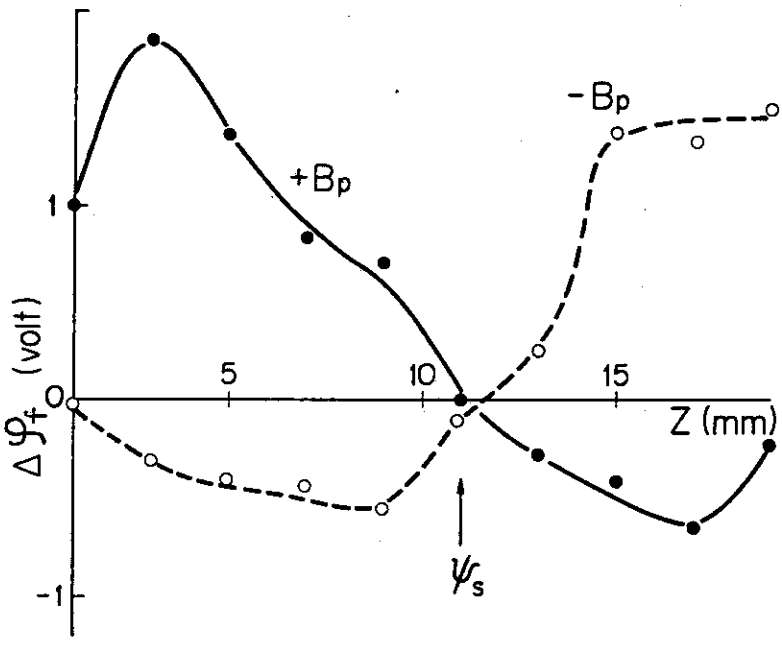

Fig. 5 Changes in floating potential $\Delta\phi_f=\phi_f'-\phi_f$ along the model support at X=-5 mm where ϕ_f' and ϕ_f are floating potential with and without the support, respectively.

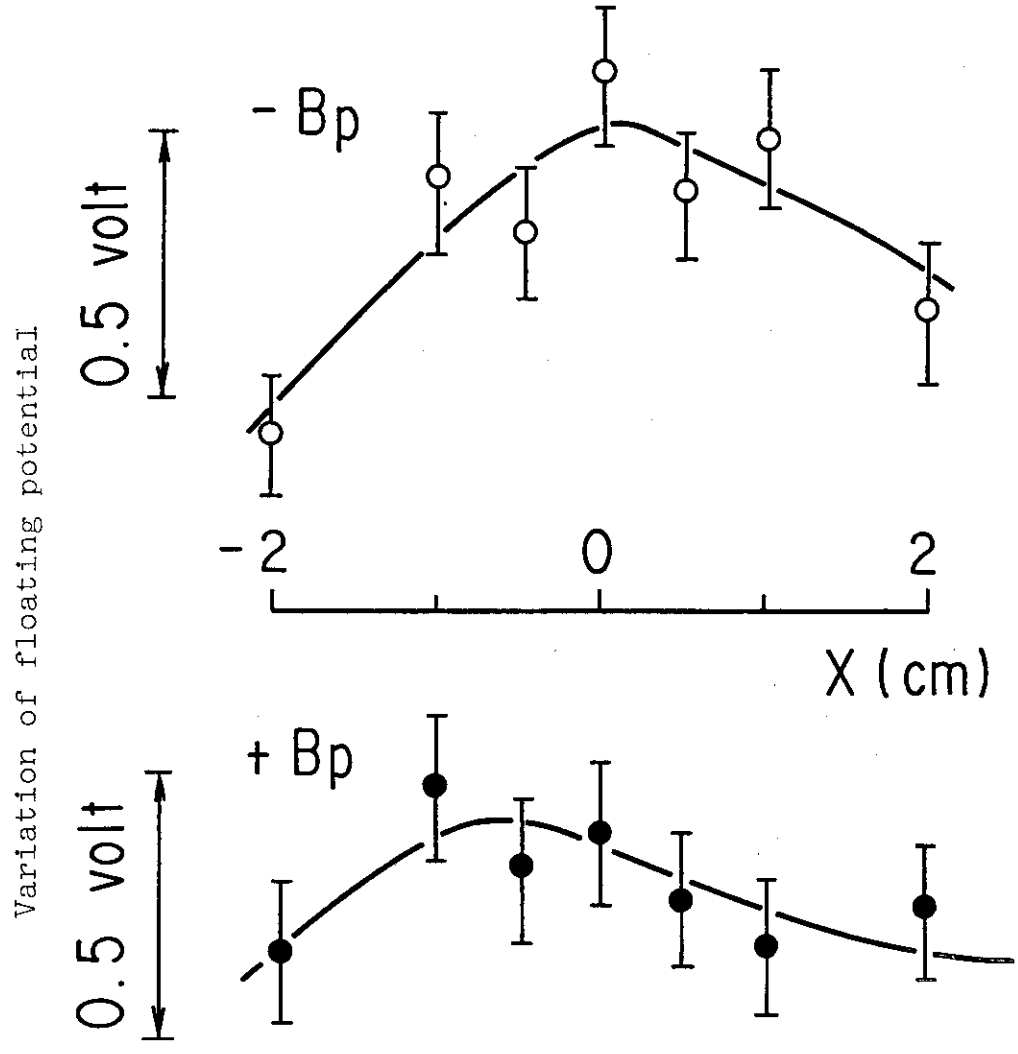

Fig. 6 Variation of floating potential near the model support (relative values) on the separatrix surface with a dependence on the polarity of B_p.

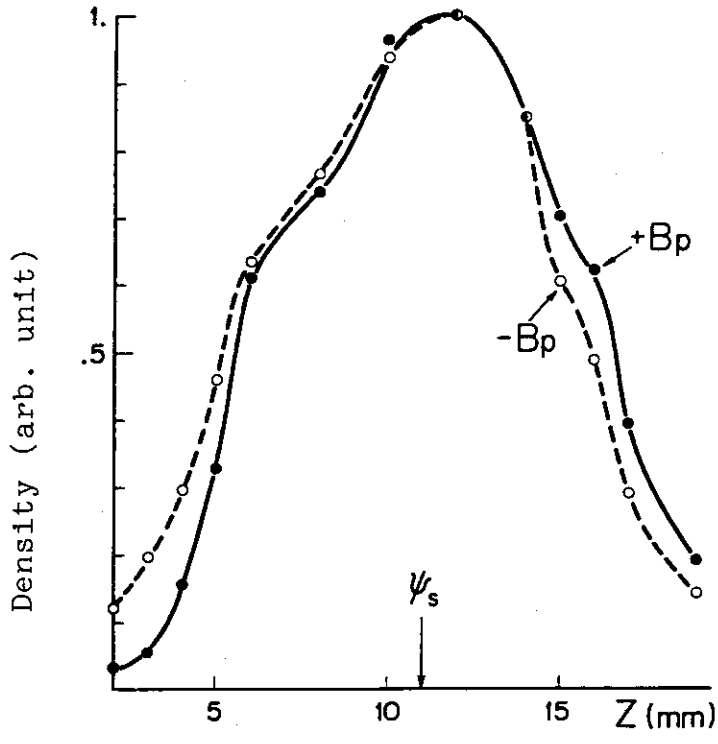

Fig. 7 Density profiles at X=-5 mm along the model support with a dependence on the polarity of B_p.

unbalance of the electric charge near the support. Since the mobility of electrons along the magnetic field line is larger than that of ions, much electrons are lost to the support than ions; and the unbalance results in.

Here, we can summarize the support induced convection as follows. The support acts as a sink of charged particles. The effect of the sink and the motions of the particles (the grad B drift motion and the motion parallel to the magnetic field) result in an unbalance of electric charge. The electric field produced by the grad B drift motion enhances the plasma loss and one appeared on the separatrix determines the loss flux pattern. Combining all of our observations, we can illustrate a support induced convection in our device as Fig. 8.

§4. Discussion

In this chapter we showed experimentally that obstacles in plasma can produce convective flow and enhance a cross-field plasma loss. The support induced convection loss has already been pointed out by experiments of Wisconsin Octopole [2] although the understanding of the result is somewhat different from ours. They stressed the role of the particle sink of the support so that the density drop across the support was explained by the sink effect. However, as to the basic role of the support, our result supported the result of the Wisconsin Octopole.

Another cause of the cross-field plasma convection which we have already known from experiments is magnetic field error. Our previous experiment [3] have shown that an artificially superposed

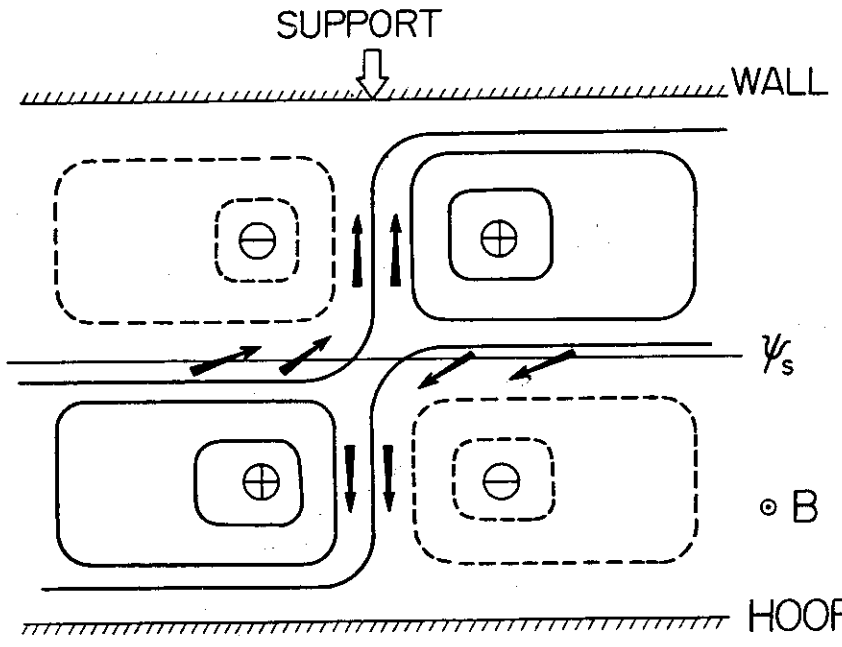

Fig. 8 Schematic diagram of support induced convection. Arrows designate the direction of the enhanced flow. Contour lines represent equi-potential surfaces.

local dipole field produces an local unbalance of charged particles which is due to escape of electrons along the stray field lines. Figure 9 shows the example of the result of the experiment. Changes in density, loss flux and floating potential as a result of the excitation of the dipole field are presented. With a similar discussion to that of previous section we can understand that the figure indicates clearly the existence of the plasma convection.

These experiments present an important knowledge that disturvance in a plasma such as supports of the internal coils or some error fields enhance plasma loss not only by the direct loss along the field line but also by forming the cross-field convective flow. A question then arises: is the convection the dominant loss mechanism in our device? We can see in Fig. 3 and 9 that the observed enhancement of the loss is at most a factor of two. The convection may not be sufficient to explain the observed anomaly in the plasma loss in JFT-1[1].

Other candidates of the anomalous loss are, as described earlier, intrinsic field errors and fluctuations. The field error of our device is caused not only by misalignment of coils but also by inhomogeneity of wall currents. Because our hexapole field is excited by a time varying (sinusoidal) curent, induced currents flow along the vacuum chamber. Many port holes of the chamber prevent the induced currents from flowing uniformly and possibly bring error fields.

In order to reduce this error field, an alminum shell whose shape was close to the hexapole contours with azimuthal uniformity was installed inside the vacuum chamber. The examination of the

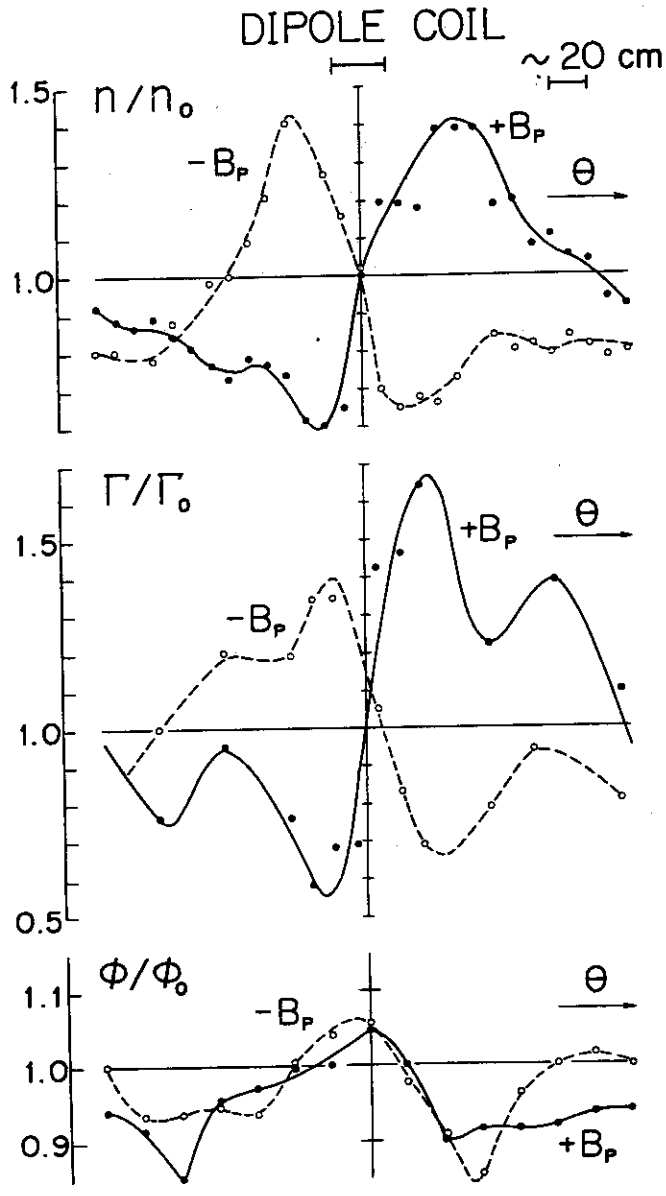

Fig. 9 Azimuthal variation of plasma density n, particle loss flux Γ, and floating potential ϕ near the outer hoop for both directions of B_p. About 5% dipole-perturbation field is present. All quantities are normalized by values at no dipole-perturbation (with subscript of 0).

effect of the shell on the overall confinement properties showed, however, that the resulting promotion was little[4]. We concluded that the actual error field of JFT-1 is not so deleterious as we have concerned.

Finally, let us discuss fluctuation in the plasma as the plasma loss mechanism. Figure 10 shows a density profile with the level of fluctuation $\tilde{n}$. As is well known, the most intense fluctuation is found at the largest density gradient. Diffusion coefficient related to the fluctuation can be estimated by the next formula [5]:

$$D = -\left(\frac{\tilde{n}}{n}\right)^2 \frac{n}{\nabla n} \frac{k_\perp T_e}{eB} \sin\delta$$

where δ is the phase difference between density and potential waves, $k_\perp$ is the perpendicular (to the magnetic field) wave number and $n/\nabla n$ represents the scale length of the density gradient. We have already known, during the course of JFT-1 experiments[1,4], necessary parameters for the relation except $\sin\delta$. If we assume $\sin\delta=1$, we obtain $D \approx 1\ m^2/s$. This value is about 100 times greater than the observed value. Therefore, the anomaly in confinement characteristics in JFT-1 may possibly be explained by the fluctuation-enhanced loss even if $\sin\delta$ is very small. In a different experiment, however, we have found a small fluctuation case without apparent promotion in the confinement [1]. A simple conclusion should be thus avoided.

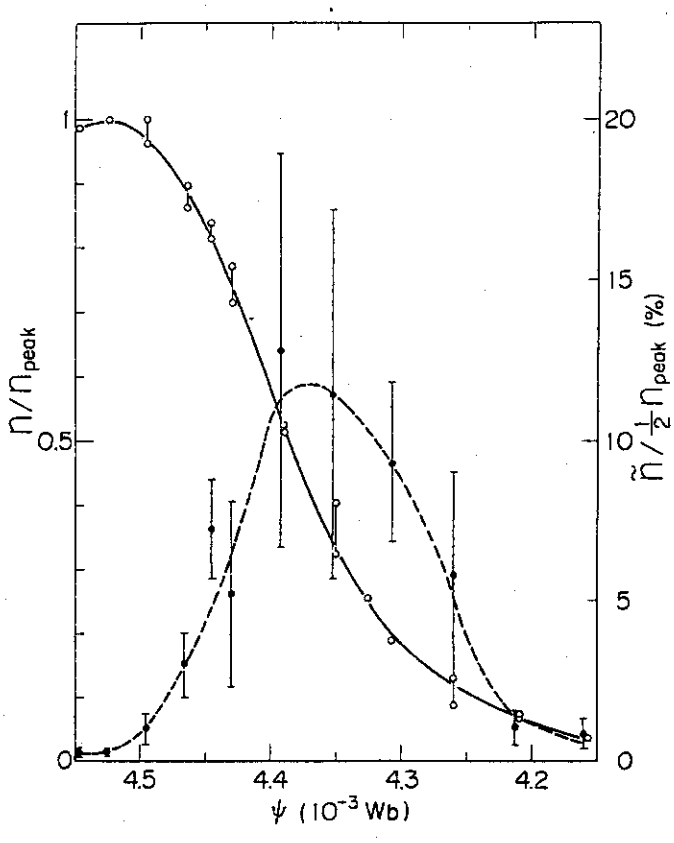

Fig. 10 Example of the fluctuation level $\tilde{n}$ (half value of the peak-to-peak) in a density profile obtained near the outer hoop.

§5. Concluding Remarks

We know that local disturbance in plasma produces a cross-field plasma convection and enhances plasma loss. The same mechanism should be also found in the tokamak device although little has been investigated up to now. A limiter, for example, which is a specific constituent in the tokamak first wall can give rise some kind of inhomogeneity. Hence, atterition should be payed to the limiter-originated disturbances. Another important fact obtained in this study is that the plasma obeys fundamental laws of plasma physics such as the grad B drift and the ExB drift although we made this study under the category of anomalous phenomena. This fact encourages us who are facing unclarified phenomena in plasma experiments.

REFERENCES

[1] S. Tamura et al., in Plasma Physics and Controlled Nuclear Fusion Research (Proc. 4th Int. Conf. Wisconsin, 1971) Vol. 1, IAEA, Vienna (1971)p75.

[2] J.A. Schmidt and G.L. Schmidt, Phys. Fluids 13 (1970) 1351.

[3] S. Tamura et al., in Controlled Fusion and Plasma Phusics (Proc. 5th Europ. Conf. Grenoble, 1972) Vol. 1, p94.

[4] H. Ohtsuka et al., Anomalous Plasma Loss in the JAERI Toroidal Hexapole, JAERI-M 5649 (1974).

[5] D.M. Meade, Phys. Rev. Lett. 17 (1966) 677.

3 PROBE MEASUREMENTS OF TOKAMAK PLASMA

§1. Introduction

To obtain reactor grade plasma it is necessary to overcome several barriers which will be encountered in the course of the plasma confinement study. The impurity problem is one of them. An estimation [1] has shown that if molybdenum, for example, which is a candidate of first-wall material is introduced as an impurity by amount of 0.1 % of the plasma, the radiation by the impurity would consume most of input power and restrict the growth of the plasma temperature. The control of impurities in the plasma is, therefore, an important subject of the present fusion research.

Divertor (magnetic limiter) is one of means to reduce impurities in a plasma. Figure 1 shows, as an example, a magnetic field configuration of JFT-2a, a tokamak with a poloidal divertor. The configuration is made by an addition of a divertor current coaxial with respect to the plasma current. The poloidal magnetic field is, hence, similar to the multipole field. Outside the separatrix, the plasma flows to the divertor region along the magnetic field line. So called neutralizer plates (divertor plates) which are subjected to received the plasma flow are set near the divertor coil. Impurities which originate from the divertor plates are forced back toward the plates again by the flow. This effect is one function of the divertor. Another function of the divertor for the impurity reduction, we expect, is so called shielding effect: impurities from the wall are

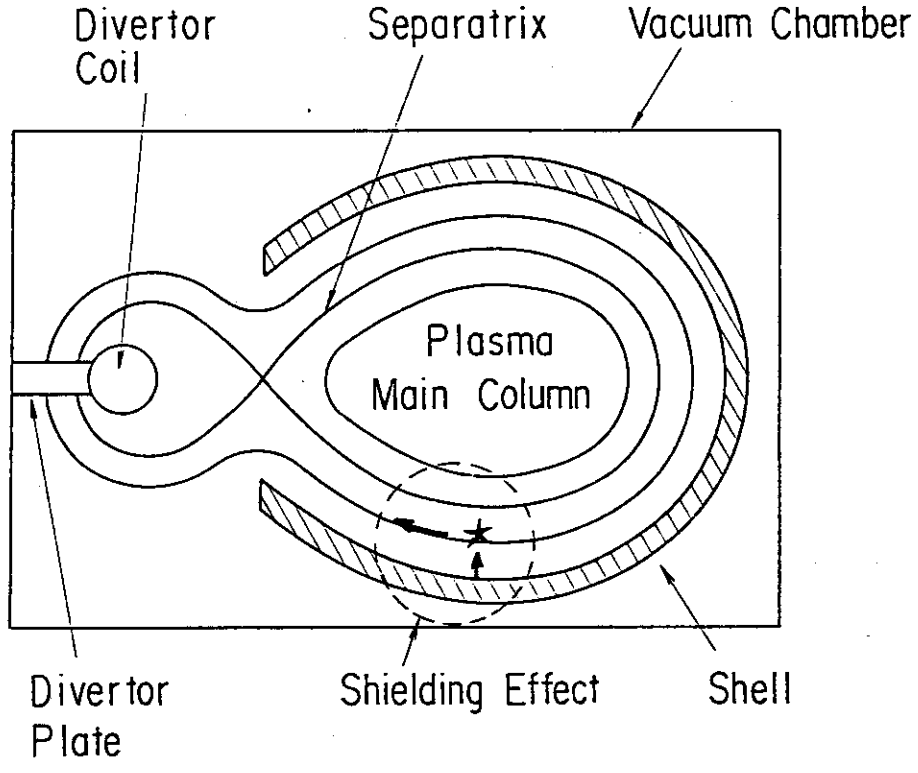

Fig. 1 Schematic diagram of a tokamak with a poloidal divertor:(JFT-2a). Contours represent magnetic flux surfaces. Shielding effect which prevents the main plasma from impurity contamination is illustrated in dashed circle: impurities originated from wall surface is ionized (marked by star) in the scrape-off layer and transferred to the divertor region along field lines.

ionized in the boundary region (scrape-off-layer) and are transported to the divertor plates by the flow.

Because the plasma-wall interaction (e.g. impurity production) is a reflex of the boundary plasma, investigations of the boundary plasma are important as well as the main body plasma. In this chapter, we describe a study of plasma behavior in the scrape-off-layer of JFT-2a.

§2. Experimental Result

JFT-2a is the first tokamak which is equipped with the poloidal divertor. Another uniqueness of JFT-2a is that copper shell which is set up usually outside the vacuum vessel of conventional tokamaks is installed inside the vessel. Shell is, in genral, aimed at stabilizing of the plasma position by image currents of the plasma current itself. To prevent induction current, the shell is devided into four toroidal sections. Furthermore, the surface of the shell of JFT-2a is covered by gold of 20 μm in thickness. The purpose of the coating is to improve vacuum characteristics. The basic machine parameters are as follows: major radius 60 cm, minor radius (on the shell surface) 10.5 × 14 cm, diverter coil radius 37 cm, number of the toroidal coils 16, toroidal magnetic field B_t up to 1T, and magnetic flux of the ion core 0.3 Vs. The present experiments were made with B_t = 1T and I_D/I_P = 0.9 (or 1.1) where I_D and I_P are divertor and plasma current, respectively. The typical plasma parameters are summarized in the inset of Fig. 2. This figure also shows the cross-section of JFT-2a. The overall characteristics of the JFT-2a plasma have been reported elsewhere [2].

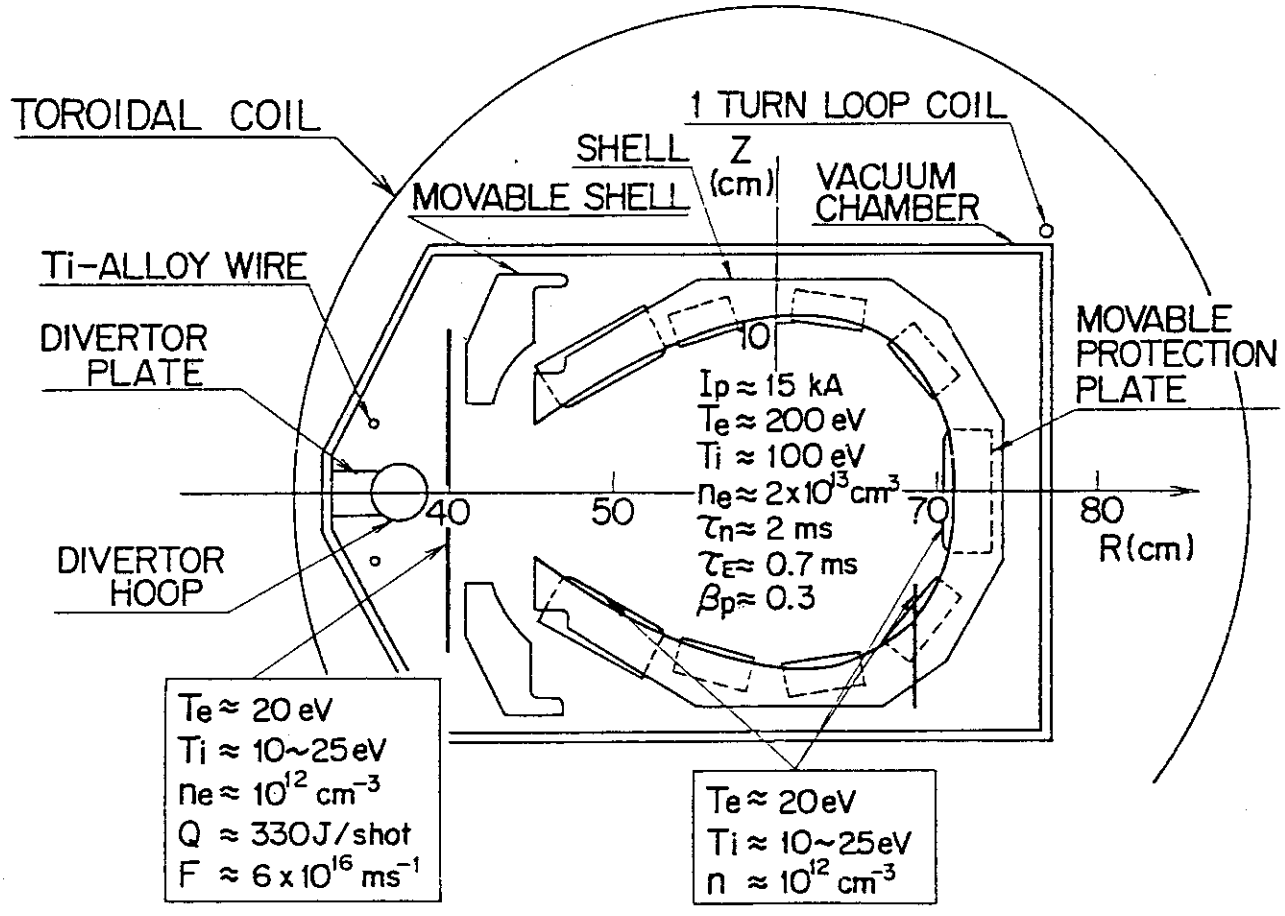

Fig. 2 Cross-section of JFT-2a. Typical plasma parameters in the main column and the scrape-off layer are summarized in the insets.

2.1 Cross-field profiles in the divertor region

Most of the electrostatic measurements in the divertor region were done at R = 40 cm being scanned in the Z direction (along the bold-faced line in Fig. 2) where R and Z represent the radial position from the center of the torus and the vertical position from the median plane, respectively. Figure 3 shows profiles at R = 40 cm of ion satutation current I_s, floating potential ϕ_f, space potential ϕ_s and electron temperature T_e at T = 10 ms (time from the beginning of the discharge). The ion temperature T_i measured with a multi-grid analyzer indicated $T_i \approx T_e$. A remarkable feature of Fig. 3 is the asymmetry of ϕ_f and ϕ_s with respect to the median plane(Z=0). It was found that the asymmetry depends on the direction of the toroidal field B_t and not on the poloidal field B_p: by reversing the direction of B_t, the profiles of ϕ_f and ϕ_s were reversed about the median plane. Taking into account the direction of the magnetic field lines and toroidal electric field E_t, we find that the most negative peak of ϕ_f always appears where electrons which are accelerated by E_t come along the field lines. This phenomenon can be attributed to an onset of suprathermal electrons which are caused by E_t and flow out from the main plasma column (see Fig. 4). Owing to the enhanced high energy part of the electron velocity distribution, the potential of the floating probe becomes more negative than that under the normal Maxwellian distribution. The asymmetry appeared because the plasma was separated by the divertor plates. The existence of the suprathermal electrons was supported lately by detection of runaway electrons in the divertor region [3].

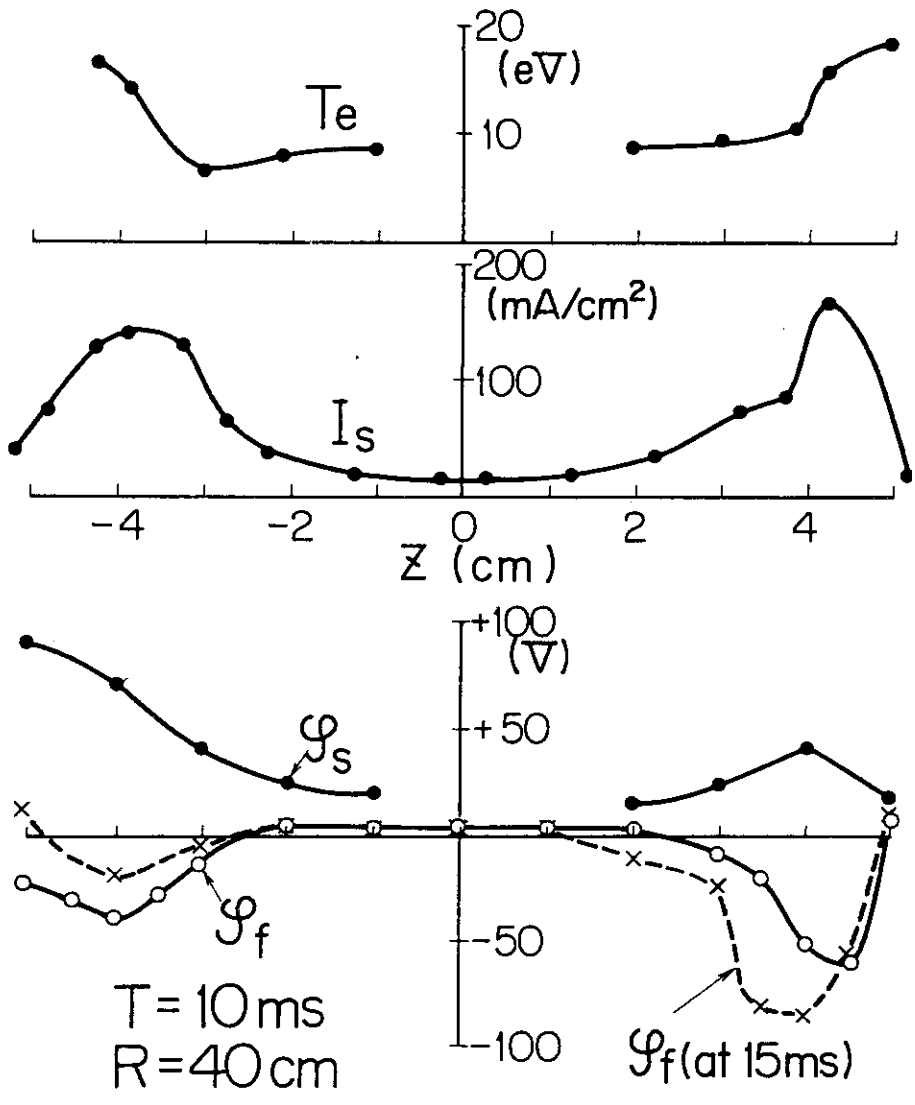

Fig. 3 Cross-field profiles of electron temperature T_e, ion saturation current I_s, space potential ϕ_s and floating potential ϕ_f obtained by Langmuir probs in the divertor region at T=10 ms.

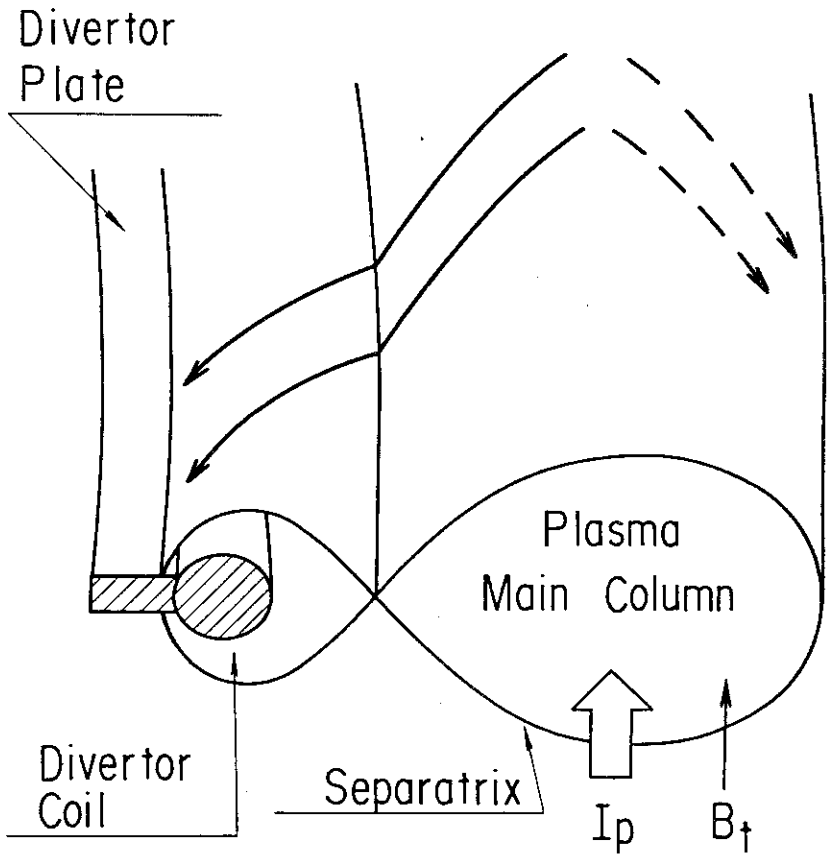

Fig. 4 Explanation of asymmetry in the floating potential. Solid lines show stream of suprathermal electrons accelerated by toroidal electric field (whose direction is the same as plasma current I_p) along magnetic field lines. When the polarity of the toroidal magnetic field (B_t) is changed, they go to the lower half one as shown in dashed lines.

2.2 Verification of magnetic limiter configuration

One of the main objectives of the early JFT-2a experiments is to clarify whether a magnetic limiter exists or not, because it is the first demonstration of the poloidal divertor operation in the world. Langmuir probes were used for this purpose. Ion saturation current in the divertor region, at R = 40 cm, was measured. In the case of I_D/I_P = 0.9, the profile had two peaks at Z = ±3 cm similar to that of Fig. 3. When I_D/I_P decreased to 0.45 no I_s peak at R = 40 cm was observed and the intensity of I_s was reduced by 1000. Figure 5 shows profiles of ϕ_f at different R in the divertor region, when I_D/I_P = 0.9. The position of the negative peaks in the profiles agrees with the separatrix magnetic surface calculated from a simple plasma model. As was described previously, the negative peak in ϕ_f is a reflex of the onset of fast electrons which came along the field lines. We can conclude from these results that the magnetic limiter configuration actually exists with I_D/I_P egual to 0.9 or greater.

2.3 Divertor efficiency and particle confinement time

Measurements of the particle flux to the divertor and to the wall were made in order to determine the divertor efficiency. To measure the particle flux to the divertor, we used a directional probe (Fig. 6) consisting of a pair of parallel plane probes which collect particles from both directions simultaneously. Ion and electron saturation current contours obtained by rotating the probe are shown in Fig. 7. Since the pattern is symmetric around θ = 0 (the direction of the field line), we can understand that the plasma flows to the divertor along the magnetic field lines

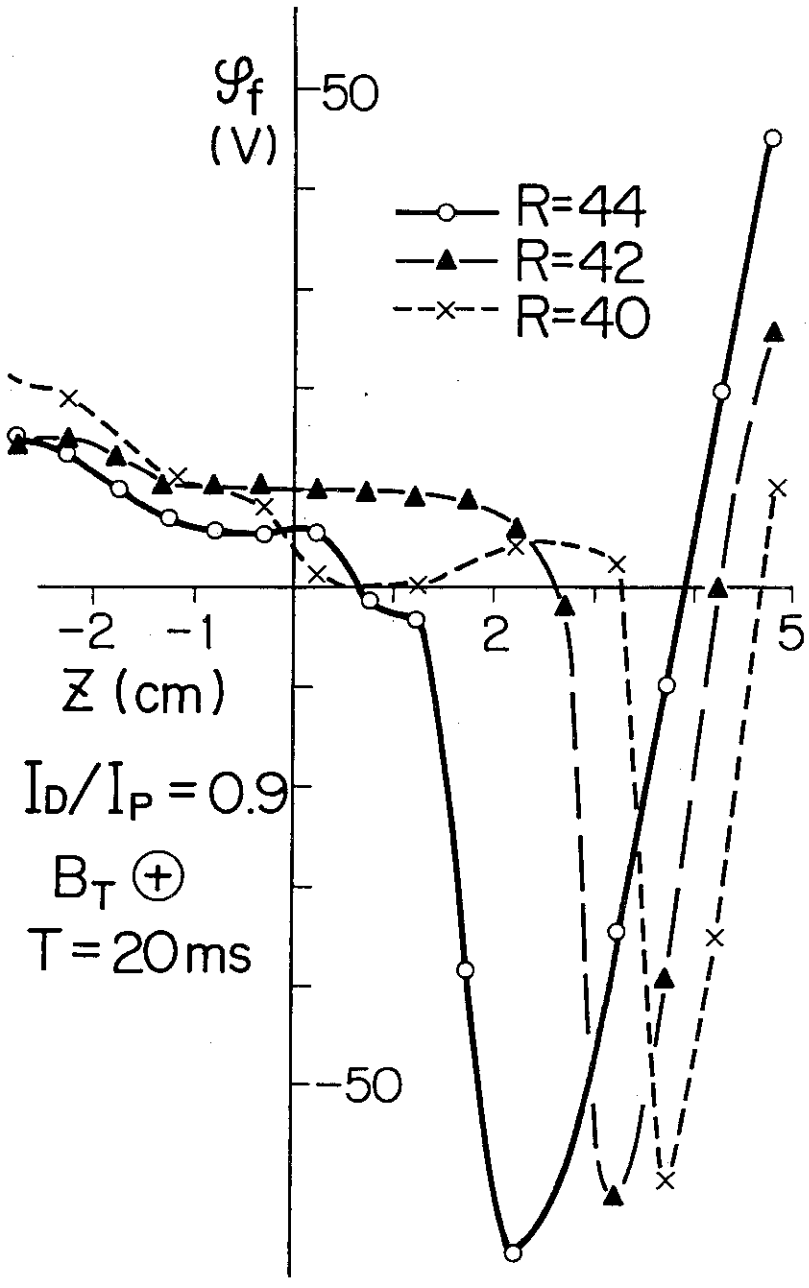

Fig. 5 Profiles of floating potential at various radial positions. In this case, I_D/I_p was set 0.9.

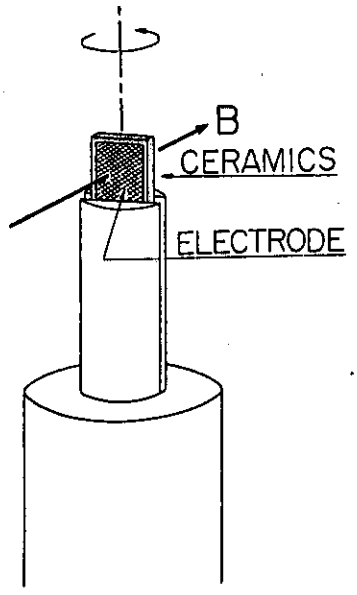

Fig. 6. A sketch of the directional probe. The probe can be rotate about its axis.

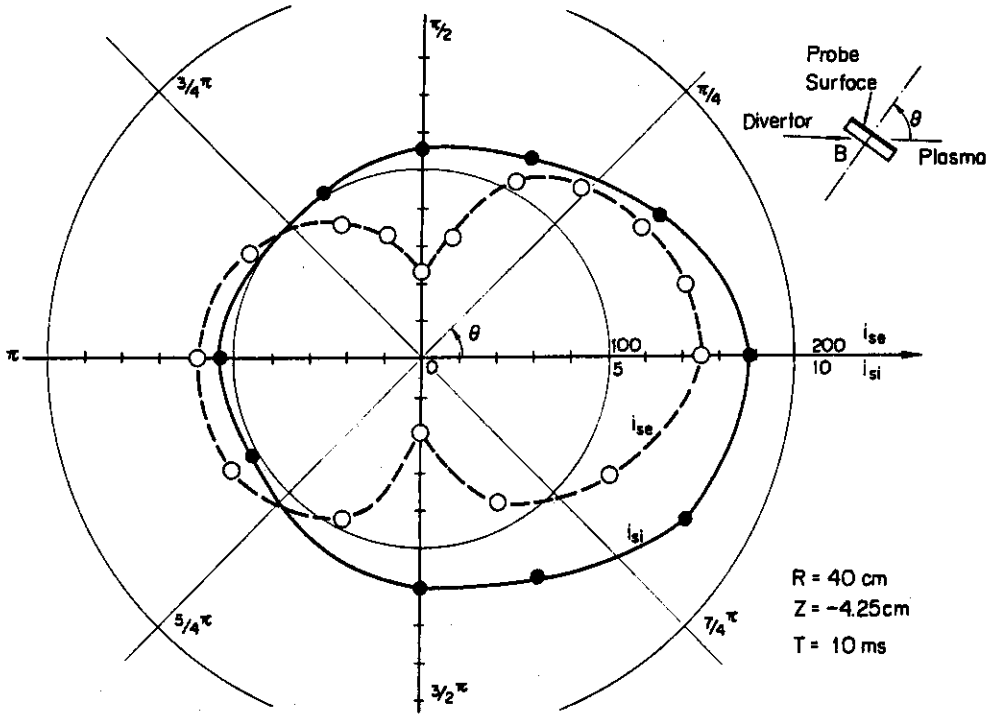

Fig. 7 Ion and electron saturation current (i_{si} and i_{se}, respectively) patterns obtained by the rotation of the directional probe in the divertor region.

and that cross-field flow (e.g. E × B flow) is less than the detectable level.

Defining J_+/J_- as the ion current density to/from the divertor region, respectively, we can calculate the particle flux to the divertor from

$$F_D = \int ds \frac{1}{2}(J_+ - J_-)\frac{B_r}{B_t} \qquad (1)$$

where $\int ds$ is the integral over the total area at R = 40 cm and B_r is the radial component of the magnetic field. Measured J_+ and J_- are shown in Fig. 8. It should be noted that a resultant reverse flow, i.e. the backward current exceeds the forward one, appears at about Z = -3 cm in Fig. 8. A discussion about this flow will be presented later.

In order to measure the charged particle flux to the wall, one of the shells was used as a collecting electrode. It was found that a large dc bias voltage on the shell prevents the initiation of the tokamak discharge. Hence, we used pulsed bias to obtain the saturation characteristics. Figure 9 shows a current vs voltage characteristic curve of a shell at a prescribed time in the discharge where the opposite electrode is the vacuum chamber. The ion currents, so obtained, to the wall and to the divertor are 84A and 8.5A at T = 10 ms, respectively. The divertor efficiency can be difined as

$$\eta = \frac{F_D}{F_D + F_W} , \qquad (2)$$

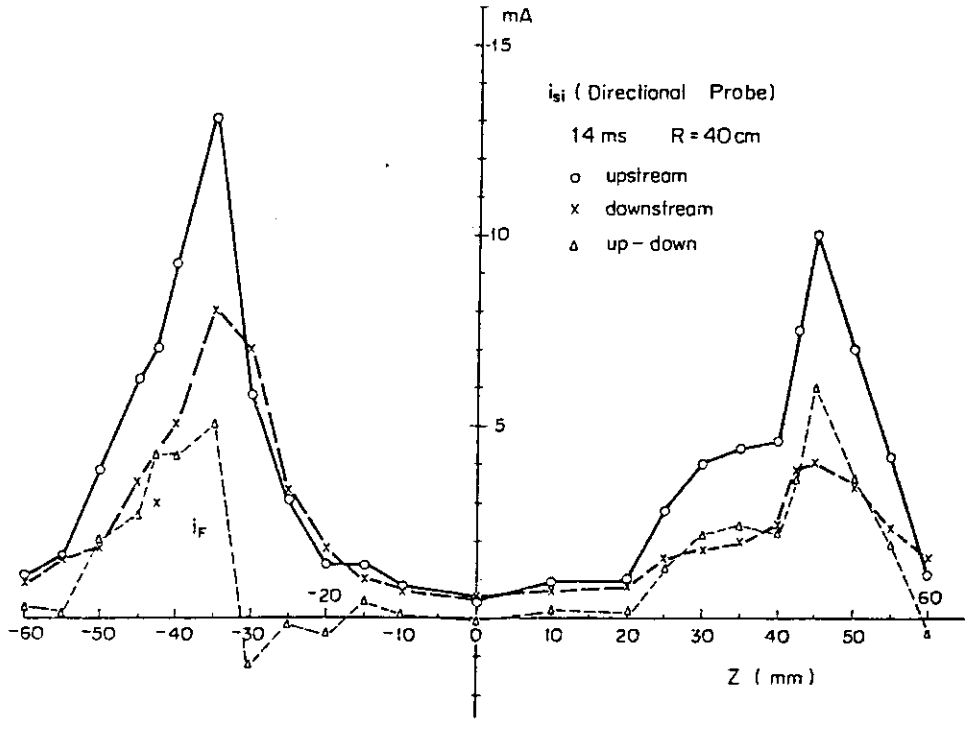

Fig. 8 Ion flux profiles in both forward and backward flow directions obtained by the directional probe at R= 40 cm. The up-stream-side probe detects the forward flow (flow to the divertor), and vice versa. The difference between the two signals shows the net flow to the divertor.

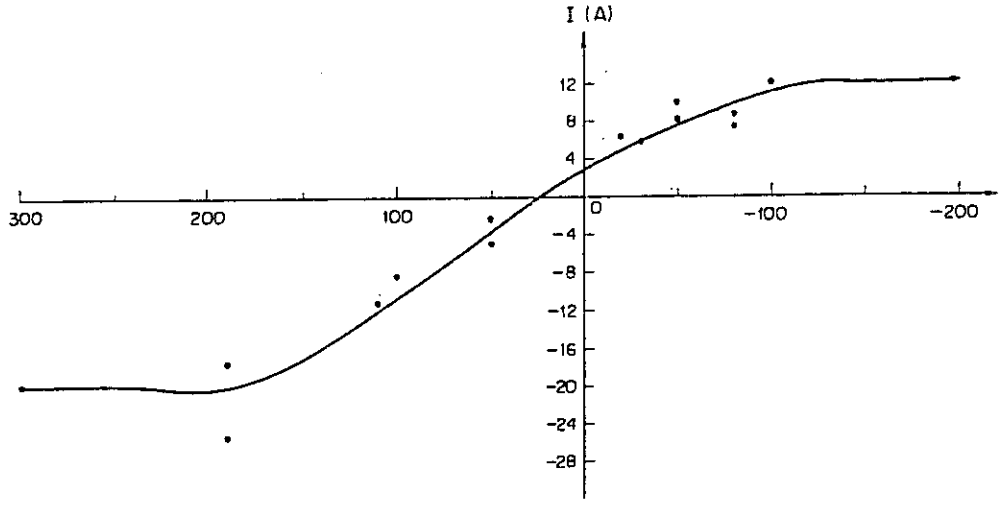

Fig. 9 Current vs voltage characteristics of a shell as a probe. The vacuum chamber is used for the opposite electrode.

where F_D is the particle flux to the divertor (including the movable shells) and F_W is the flux to the shells (including the limiters). Hence, η is estimated to be about 0.1.

Next, we describe the particle confinement time τ_n. Knowing the total particle flux F from the plasma main column and the total number of confined particles N, we can estimate τ_n, viz:

$$\tau_n = \frac{N}{F} \tag{3}$$

The value of N was known with the microwave interferometer. Time variation of τ_n from N/F is shown in Fig. 10 together with τ_n from the H_α-line measurement. In the first half of the discharge, values of τ_n agree with each other. The discrepancy in the latter half is not yet fully understood, but may be due to impurities.

2.4 Reverse flow and drift motion of ions

In this subsection, we discuss the reverse flow in the divertor region which is found in Fig. 8. An understanding of trapped particle orbits may explain this phenomenon. A cross section of a typical trapped ion orbit near the divertor coil is shown in Fig. 11. An ion which starts from point A makes an excurtion through BCDE. The deviation of the orbit from the original flux surface and the reflection are due to the grad B drift and the mirror effect (because $B \propto 1/R$), respectively. At the mirror point C, the motion is reversed in the toroidal direction as well as the poloidal one. Hence, the motion of the reflected ions constitutes the back stream. The reverse flow at

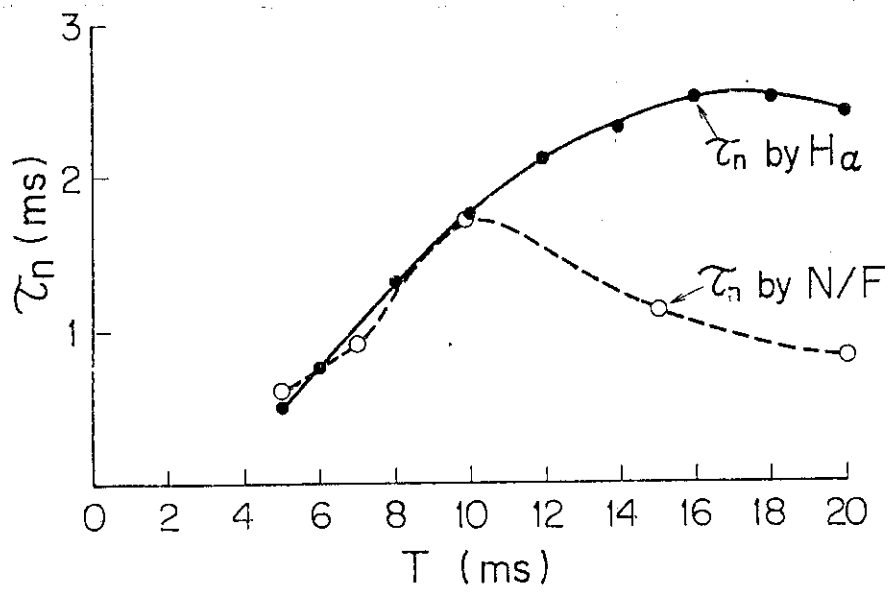

Fig. 10 Particle confinement time τ_n obtained by the electrostatic probe method. τ_n by using the optical method (H_α-line) is also shown in solid line.

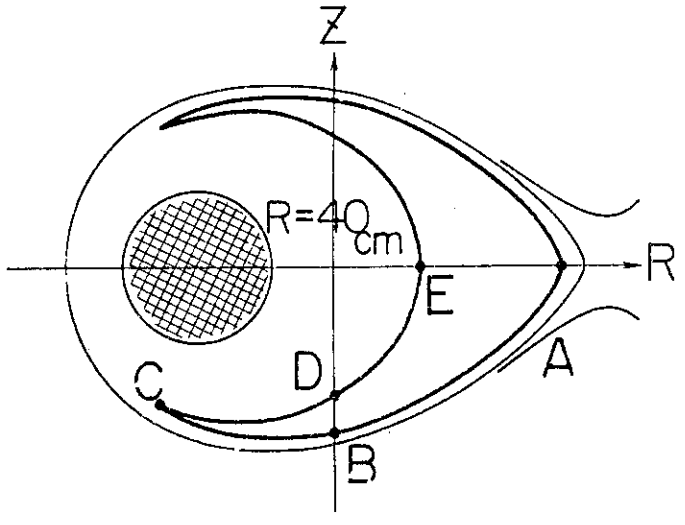

Fig. 11 Cross-section of typical drift orbit of a trapped ion in the divertor region. The excurtion is made through ABCDE.

D results when the reflected particle flux exceeds the forward flux (flux in the direction of ED). This situation is easily realized because the plasma density at A is, usually, much higher than that at E. This mechanism is reminiscent of so called bootstrap current [4], although the two situations are different. Details of the particle orbits, however, are complicated because effects due to the toroidal electric field E_t and collisions are not negligible. By taking accont of E_t, detrapping due to acceleration in the torodial direction should occur; that results in the escape of almost all the particles from trapping. On the other hand, collisions impede this acceleration. Therefore, the observed backward flow may be explained by the drift motions of ions which are back-scattered due to mirror reflection and/or collisions. The position where the backward flow was observed changed from Z = -3 cm to Z = +3 cm when the direction of the B_t was reversed. This result is consistent with the foregoing explanation.

2.5 Measurement of flow velocity

Measurement of the flow velocity in the divertor region is important for the estimate of the divertor efficiency. In a sense, we have implicitly taken into account the flow velocity in Eq. (1). However, if the shadow effect of the probe itself is not negligible, Eq.(1) is incorrect. Let us assume that, when its surface is parallel to the flow, the directional probe collects ions such that $J_o = \frac{1}{2}nC_s$ where n is the plasma density and C_s is the sound velocity. This assumption is valid if $\lambda_D \ll \rho_i \ll r_p$ where λ_D, ρ_i and r_p are the Debye radius, ion Larmor radius and

probe size, respectively. On the other hand, when its surface is perpendicular to the flow, the current density may be written as $J_+ = \frac{1}{2}nC_s + nV_f$ where V_f is the flow velocity. Thus we can obtain the flow velocity, corrected for the shadow effect, by measurement of J_o and J_+. Note that in this experiment, the result showed the shadow effect to be negligible in our plasma. An excellent method for measureing the flow velocity has been used in the FM-1 device [5]. They excited a wave in the plasma and determined the flow velocity from its time of flight. However, in the JFT-2a plasma, excitation of ion sound waves in the scrape-off layer is difficult because $T_i \approx T_e$. Our results $V_f = (0.3 \sim 0.5)C_s$, using the directional probe, agree with those of FM-1 where $V_f = 0.3C_s$.

2.6 Diffusion coefficient in the divertor region

The cross-field diffusion coefficient in the scrape-off-layer is closely related to the divertor efficiency. The diffusion coefficient D in the divertor region can be estimated experimentally by measuring two density profiles at different radial positons. The profile $n_1(Z)$ (see Fig. 12) is considered as a source distribution so that we can compare the measured profile $n_2(Z)$ with the calculated one. Assuming simple one dimensional diffusion, we obtain the following relation;

$$n_2(Z,t) = \int G(Z,t,Z',t_o)n_1(Z',t_o)dZ' \qquad (4)$$

where

$$G(Z,t,Z',t_o) = \frac{1}{\sqrt{4\pi D(t-t_o)}} \exp\left\{-\frac{(Z-Z')^2}{4D(t-t_o)}\right\}$$

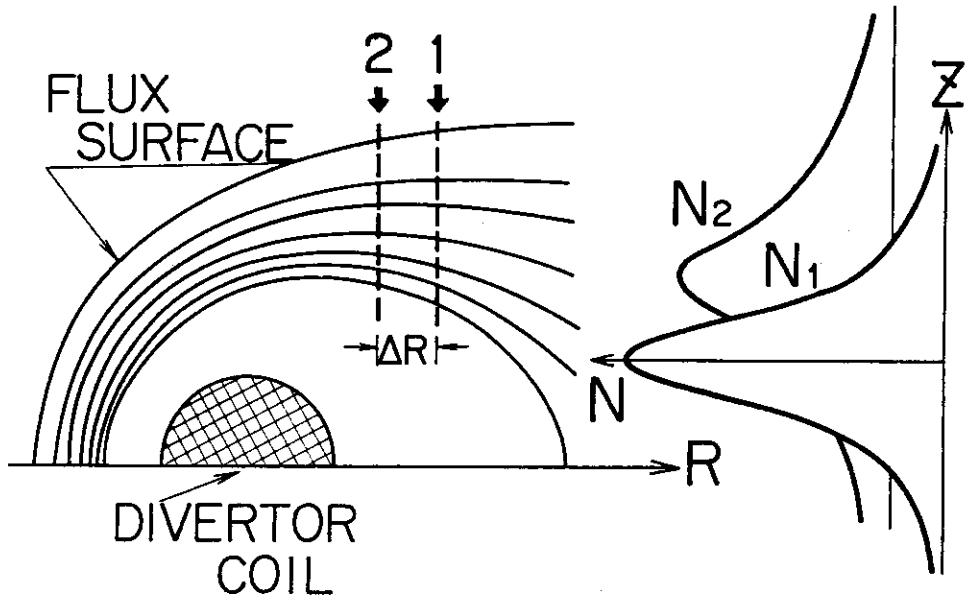

Fig. 12 Measurement of diffusion coefficient in the divertor region. Density profiles N_1 and N_2 are obtained at different R. With pertinent consideration of the magnetic field, comparison between N_1 and N_2 gives the diffusion coefficient.

The difference between the calculated and the measured $n_2(Z)$ is minimized mumerically by adjusting the value of D. Since the two profiles are measured simultaneously, the time variable t in the Eq. (3) should be replaced by $\frac{\Delta R B_t}{V_f B_r}$, where ΔR is the distance between the two probes. Figure 13 shows an example of the measured profile. The magnetic flux density was adjusted to be uniform so that the Eq. (3) could be used. In the calculation, we took artificially the outer half of the profile with respect to the separatrix (at the peak of the proile) because the inner half one is somewhat different. The value of D was found to be of order of the Bohm diffusion, defined by $D_B = \frac{T_e}{16eB}$, with an assumption of $V_f = 0.5C_s$. Uncertainty in the V_f evaluation corresponds to a factor of 2.

Figure 14 shows fluctuation level of the ion saturation current in the divetor region. It is found that the flucturation is localized in the region of greatest density gradient. The large diffusion coefficent may be, at least partly, due to this fluctuation.

§3. Conclusion

During the course of this study, various measurements of the boundary plasma using electrostatic method have been presented. The fruits of this study may be summarized as follows.

1) This study presented the first result of measurement of the tokamak boundary plasma. It added knowledge of the scrape-off-layer to that of the main plasma column.
2) The results successfully demonstrated the usefulness of the

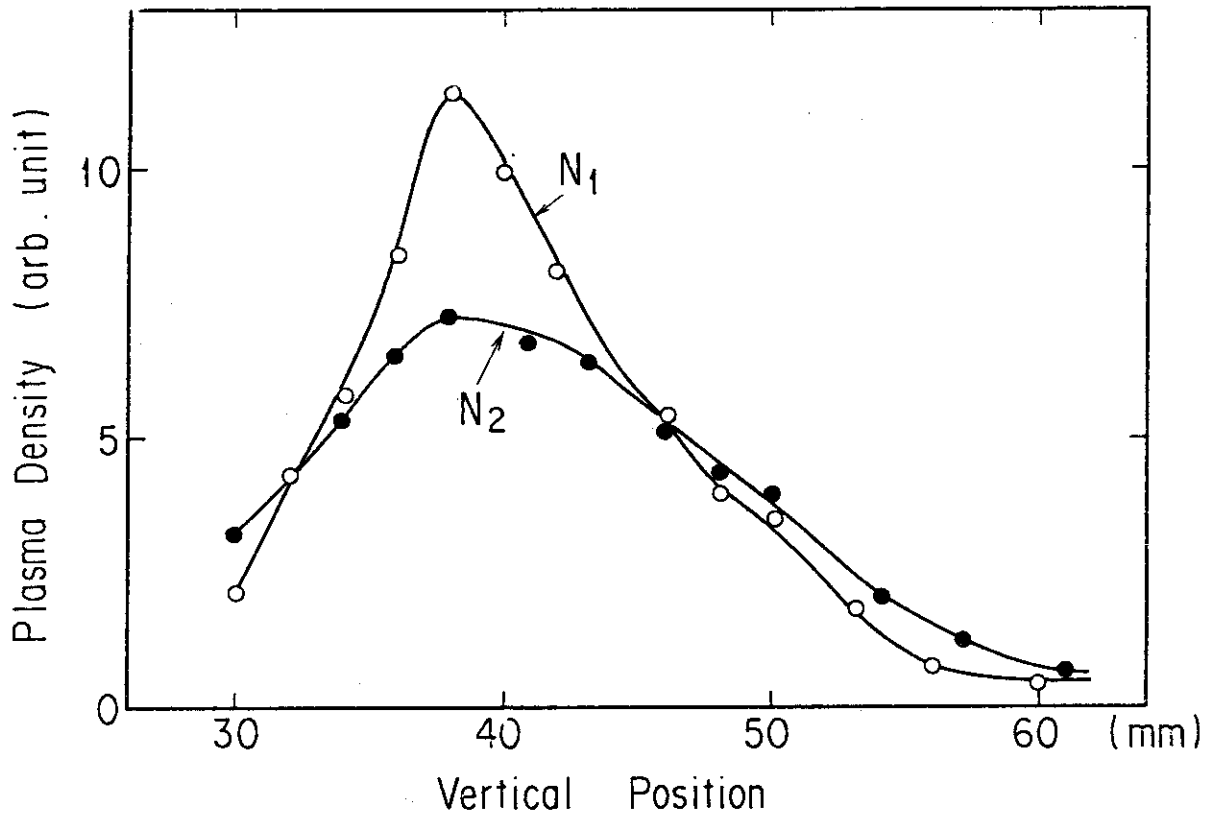

Fig. 13 Density profiles at different radial position in the divertor region for an estimation of the diffusion coefficient. The reduced distance between two probes are about 20 cm whereas actual separation is 10 mm. The abscissa is adjusted so that the magnetic flux density is uniform.

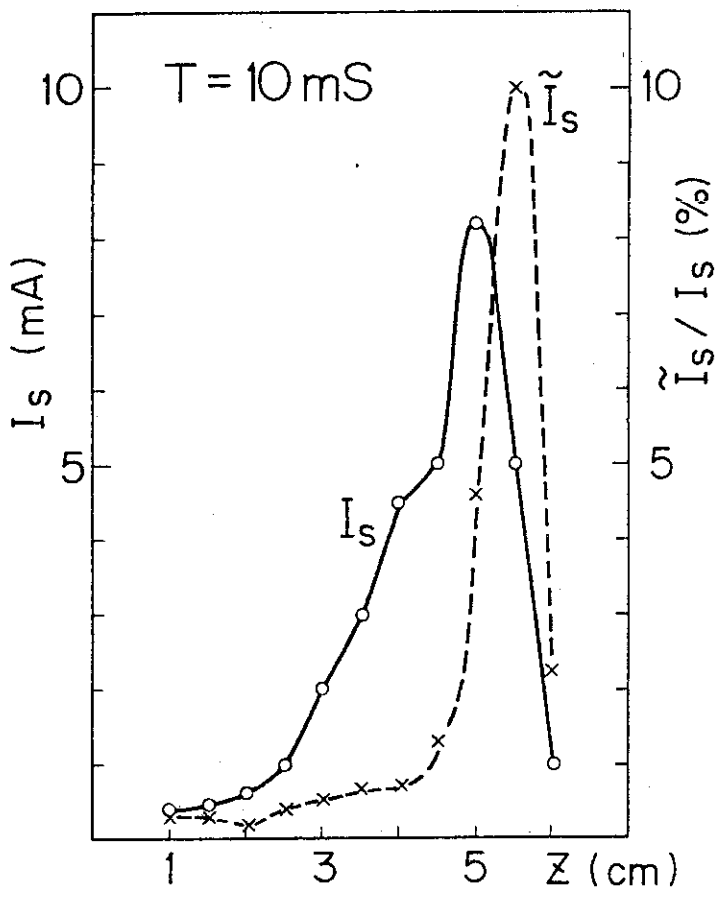

Fig. 14 Fluctuation level $\tilde{I}$ in the ion saturation current profile at R=43 cm. The frequency range is 50 kHz-200 kHz and typical wave-length is about 1 cm.

electrostatic method.

3) Especially, the method contributed to the divertor study of JFT-2a which is the first tokamak equipped with the axisymmetric divertor. The existence of the divertor configuration and the function of the divertor were exhibited.

4) Unexpected plasma behavior , i.e. a reverse flow in the divertor region was found and was interpreted by the drift motion of ions. This result recalles us to the previous chapter where we discussed anomalous plasma loss in terms of also the drift motion. Lately, we will meet again the drift motion of the boundary plasma which relates to the plasma-wall interaction.

REFERENCES

[1] R.V. Jensen et al., Nucl. Fusion 17 (1977) 1187.

[2] Y. Shimomura et al., Phys. Fluids 19 (1976) 1635.

[3] S. Yamamoto et al., Nucl Fusion 18 (1978) 205.

[4] R.J. Bickerton, J.W. Connor and J.B. Taylor, Nature, Phys. Sci. 229 (1971) 110.

[5] H. Hsuan, M. Okabayashi and S. Ejima, Nucl. Fusion 15 (1975) 2.

4 STUDY OF ARCING

PART I: ARCING AS AN IMPURITY SOURCE

§1. Introduction

When a plasma contacts with the container wall, there arises a possibility that the plasma produces arcing on the metal surface. It is called unipolar arcing [1] because no anode electrode exists seemingly within the vessel whereas the metal surface acts as the cathode. Considering the plasma as the anode, however, we can understand that unipolar arcing is not so different from conventional vacuum arcing: that is, arc voltage is maintained by the sheath potential given by the plasma energy and the arc current is sustained by the electron flow from the plasma to the metal wall. This situation is illustrated in Fig. 1.

Arcing first became of interest to fusion researches when it was realized that arcs played a dominant role in introducing impurities into ZETA exteriment [2]. Arcing was largely forgotten, however, with the demise of ZETA. Recently, interest in arcing has been revived in the tokamak experiments because of the evidence of arc tracks on the first wall [3]. Arcing melts the surface and evaporates its material. It was condidered that the volume of materials ejected from an arc spot can produce enough impurities to give rise deleterious effects to the plasma. However, little has been known about arcing on the tokamak first wall so far.

In this part, we describe results of an experimental study of arcing in JFT-2 tokamak. In the following two sections, we

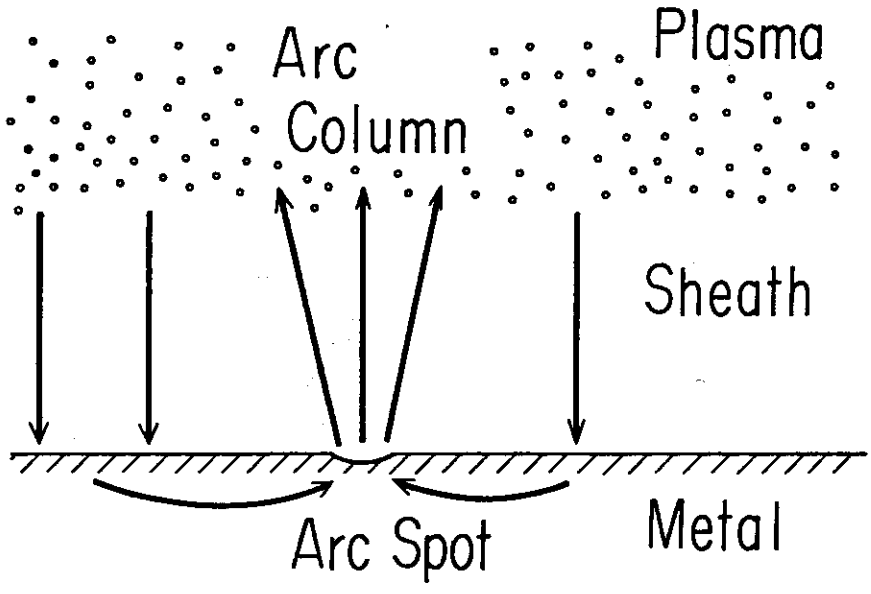

Fig. 1 Structure of unipolar arcing. The arc current is generated by secondary-electron emission at the arc spot. Closed circuit of electron current (indicated by arrows) is formed by high energy electrons in plasma which overcome the sheath potential and flow into the metal cathode.

present the experimental set-up and the observation of arc tracks peculiar to the tokamak first wall. In §4, a method of the real time detection of unipolar arcing is stated with emphasis on the most reliable way to identify arcing. The results made it possible to know plasma parameters at the initiation periods of arcing. Measurements of plasma parameters which clarify the cause of the arc initiation are presented in §5. In §6, we also discuss an asymmetry of arc tracks which is pointed out in §3. Finally, in §7, we summarize the results of the experiments. An important conclusion that we may not necessarily be anxious about arcing as a fatal impurity source in future tokamak is presented.

As is shown in §3, the motion of arcs on the tokamak first wall, which is known as the retrograde motion, is related to an amount of impurity release. In this point of view, an analysis of the cause of the motion is made. The retrograde motion has been observed in the first decade of this century. Because of the strangeness of the phenomena it has absorbed much interest of scientists in this field. Several tens of theories which intended to explain the cause of the motion have been proposed so far. These theories, however, seems to have not yet succeeded in explaining the whole mechanisms. Apart from the fusion research, the problem draws our interest. We propose a new theory which shows good agreement with the known phenomena. The new theory is presented in part II of this chapter.

§2. Experimental set-up

JFT-2 is a conventional tokamak with circular cross section. Basic machine parameters are listed in Table 1. For the study of

Table 1 Parameters of JFT-2

Machine Characteristics	
Major radius	$R = 90$ cm
Limiter radius	$r_L \leq 28$ cm
Wall radius	$r_W \leq 31$ cm
Toroidal magnetic field	$B_t \leq 1.6$ T
Material Wall	Stainless Steel
Limiter	Stainless Steel/ Molybdenum
Wall conditioning	bakable 350°C T_i-gettering TDC[a)]
Parameters of Joule-heated plasma	
Plasma Current	$I_p \leq 160$ kA
Central electron temperature	$T_e = 0.6 - 1.0$ keV
Central ion temperature	$T_i = 0.25 - 0.4$ keV
Mean electron density	$\bar{n} = 1 - 3 \times 10^{13}$ cm^{-3}

a) Taylor type discharge cleaning

arcing, we set up a real time observation system by using a surface analysis station. A schematic diagram of the surface station and the set-up are shown in Fig. 2. The surface station consists of Auger Electron Spectroscopy (AES), Scanning Electron Microscope (SEM) and a driving mechanism with which samples are transferred from the first wall to the analyzers. This system enables us to make in situ analysis of the sample surface. The real time arc detection was made by a combination of following means. Monitoring sample current: this was intended to exhibit directly the arc current. In order to do so, the sample was connected to the wall with 0.1 ohm resister. Both positive and negative bias voltage with respect to the wall was applied in order to measure the electron or ion current from the plasma to the sample. Detection of the light emission from the sample surface: this was provided because arcing might be accompanied with the light emission. A system which consisted of a photo-diode, a mirror and a vacuum-tite window was used to catch the light emission. Monitoring the plasma near the sample: this measurement was intended to relate the plasma parameters with the arcing phenomena. For this purpose a Langmuir probe was used. Furthermore, detection of hard X-ray, which is an index of a production of run-away electrons in the plasma, was made with a NaI scintillator with a photomultiplier.

§3. Observation of arc tracks

By the visual inspection we can recognize, usually, whether arcing occurred on the tokamak first wall or not. A typical example of arc tracks of the tokamak first wall is shown in Fig. 3.

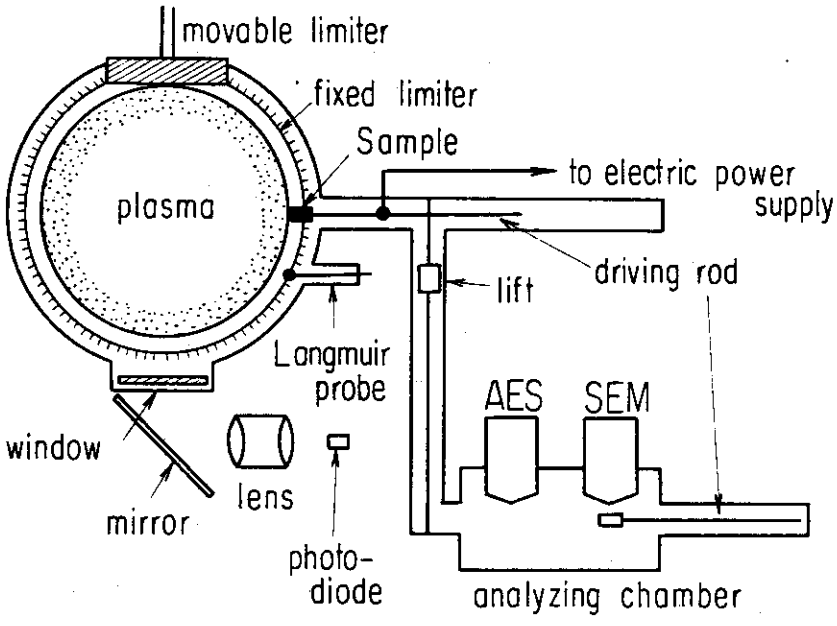

Fig. 2 Schematic diagram of the experimental set-up.

A limiter, so called rail limiter, used in JFT-2 is shown. White traces as if they were made by sweeping a broom are the arc tracks. Characteristic features of the tracks obtained from a brief look are as follows. The figure of the tracks looks like ribs of a fan. The length of the tracks extends up to 5 cm. The number of tracks left on the surface is asymmetric as to the toroidal direction: namely, much tracks is observed on the ion side of the limiter (right hand side in this figure) than the electron side, here ion and electron side are defined as up- and down-stream sides of the plasma current, respectively. The asymmetry of arc tracks can also be found on sample surfaces as shown in Fig. 4, which was exposed to the boundary plasma of JFT-2. This figure shows arc tracks on the same sample viewed from directions opposite with each other. It is noteworthy that the figure of the tracks on the sample is straight but on the curved surface it is curved as shown in Fig. 3 and lately in Fig. 13.

Arc tracks on the surface perpendicular to the magnetic field appear different from ones presented so far. Figure 5a/5b show the tracks on surfaces, which belong to the same sample, parallel/perpendicular to the magnetic field, respectivley. The spots are a character peculiar to the perpendicular surface. On the contrary, on surfaces parallel to or taking an oblique angle to the magnetic field the tracks appear. It is reasonable to consider that arc moves on the surface when the angle between the surface and the magnetic field is appropriate. The movement results in the elongation of the life time of arcing. Therefore, the volume of surface material ejected by one arcing is very different depending on the angle. This point of view is, needless to say,

Fig. 3 Typical example of arc tracks left on a limiter (stainless steal; 18 cm x 5 cm).

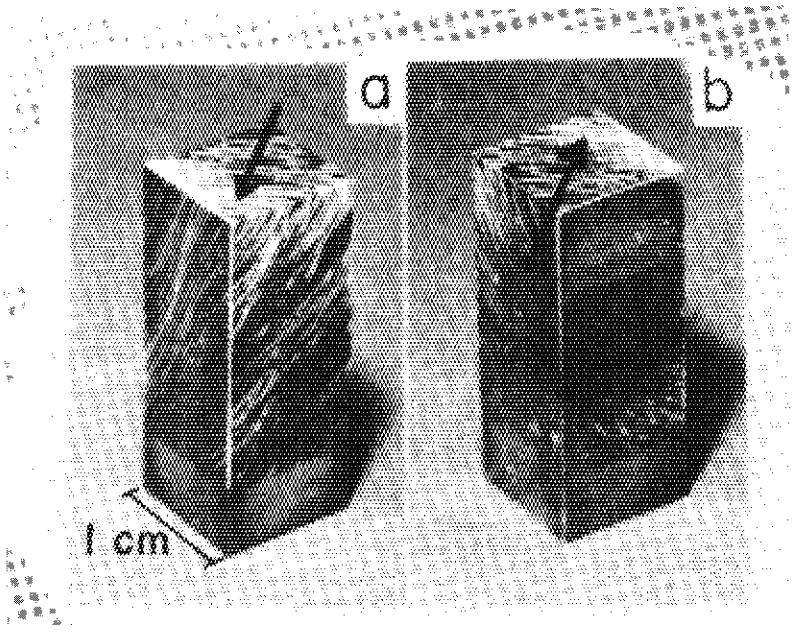

Fig. 4 Asymmetry of arc tracks on a sample surfaces; a) ion side, b) electron side of the same sample. Arrow indicates magnetic-field direction parallel to top surface.

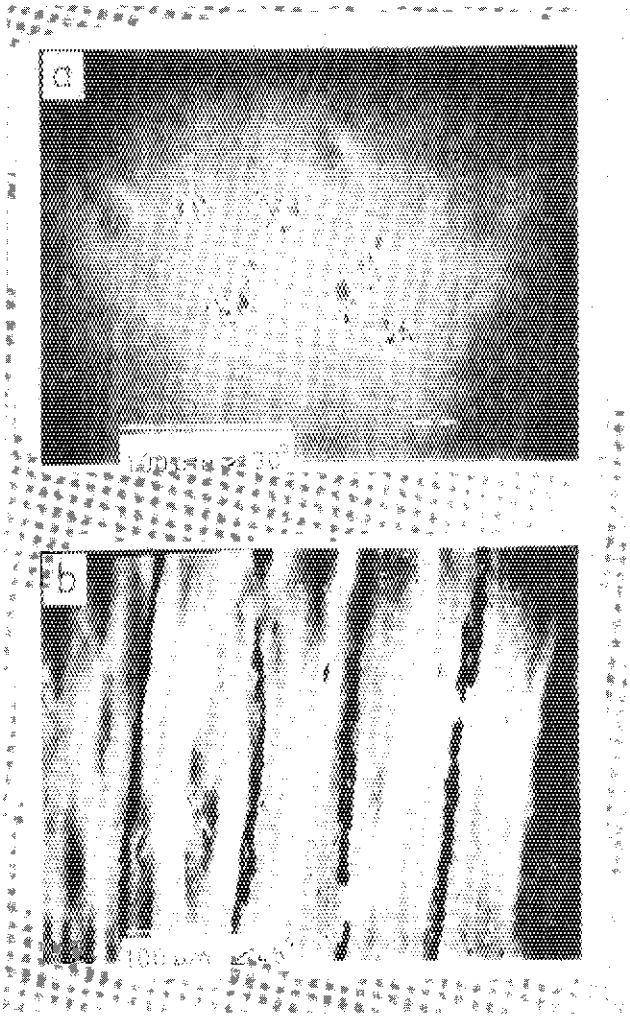

Fig. 5 Two types of arc track on a sample surface; a) perpendicular/ b) parallel to the magnetic field. The angle between the surface normal and the SEM electron beam is 30° for a) and 45° for b), hence the horizontal scale should be read with the correction.

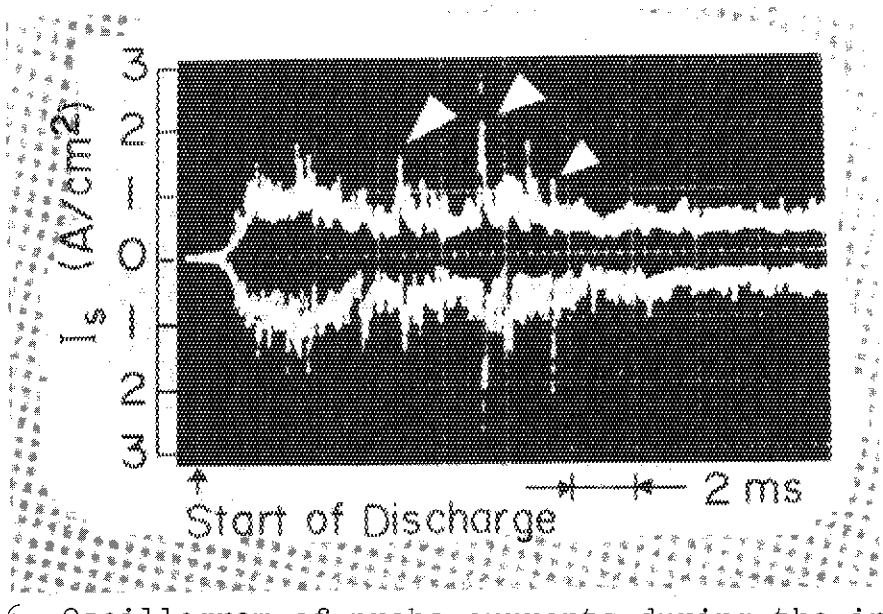

Fig. 6 Oscillogram of probe currents during the initial phase of two discharges, showing typical spikes (indicated by arrows) and their reproducibility. One of them is shown up-side down.

very important for the fusion devices. For example, in Fig. 5a the size of the spot is typically 10-30 μm in diameter while the size of the tracks is up to 10 mm or more with 10-30 μm in width. The ratio of the erosion rate, namely the amount of ejected impurity, is 10^2-10^3, assuming that their depth is equal.

The motion of arcs in the magnetic field is usually called the retrograde motion. The name comes from the fact that arcs move in just inverse direction of the J×B force (Ampere's law) where J is the arc current which flows from the plasma to the surface and B is the magnetic field. This phenomena has been first pointed out by Stark at the beginning of this century[4]. However, the mechanism of this motion has not been clarified yet. In view of the importance for the fusion research, we intend to analyze the phenomenon theoretically. The analysis is described separately in part II of this chapter.

§4. Method of arc detection

In this section, we consider problems which concern with the detection of arcing by a real time method. On the basis of the result, we can proceed the arguement about the cause of arcing on the tokamak first wall. Figure 6 shows wave forms of the ion saturation current obtained by the probe during initial unstable phase of plasma discharges. In this figure signals of two subsequent descharges are shown (one of them is shown up-side down). Large spikes in the figure (indicated by arrows) are a reflex of the disruptive instability: that is, a sudden outward shift of the plasma column results in the increase of the probe

current. In general, initial phase (current rising phase) of a discharge is always unstable in tokamaks. It has already been pointed out in our previous studies [5,6] or others [7,8] that arcing in the tokamaks ocuurs at periods of the disruptive instability and not during a stable plasma discharge. Therefore, in the following, we shall focus our interests on the initial phase of discharges. The preprogrammed start-up of JFT-2 discharges has fixed wave forms of the control fields. Especially, the current for the vertical field, which stabilizes the plasma position, is supplied by rectifying commercial ac lines. It was found that timing of the instability coincides with the commutation time of the thyrista rectifiers. This character reflects to the reproducibility of the timing when the spikes appear. Figure 6 shows the spikes are well reproducible. In these circumstances, we have to identify signals of arcing in the sample current (arc current) and in the light emission on the surface.

The identification is basically difficult. When the plasma onset comes a pulsive sample current similar to the probe current flows. Arcing whose occurrence coincides with the plasma onset also accompanies with current, i.e. arc current. That is to say, both the plasma onset (the cause) and arcing (the result) appear in the sample current as a pulsive signal. Similar confucion also exists in the detection of light which is due to arcing or the hydrogen related radiation. This situation gives rise to a criticism that recent understanding of the real time observation method [7,8] seems to be somewhat uncertain. They simply considered the pulsive signals arcing.

Figure 7 shows oscillogram of the ion/electron current of

the sample obtained by biasing the sample negatively/positively, respectively. The double probe signals which monitor the plasma density near the sample are also shown. Both ion/electron currents approximately agree with the density fluctuation except for negative spikes in the electron current (indicated by arrows). The negative spikes are possibly an index of arcing because the direction of the arc current is opposite to the electron current. Positive spikes in the ion current might also be the results of arcing. However, because both direction of the current of ion flux and arcing are same, we can not draw such conclusion from the signal solely.

Light signals from a sample during initial phase of plasma discharges are shown in Fig. 8. Signals of the first three successive exposures are demonstrated in the figure. The signal changed shot by shot: light spikes decrease with the number of plasma discharges. Since the plasma onset is reproducible, the signals must not simply be the hydrogen radiation. Arcing or light impurity desorption may show such change because the surface condition varies shot by shot by the plasma impacts. This phenomenon is known as the conditioning effect. After the exposure, we found arc tracks on the sample surface (e.g. Fig. 4). Therefore, it is natural to attribute the spike signals to arcing.

In summary, for the real time identification of arcing we should like to stress the necessity of careful investigation by using a combination of several detection techniques. We presented here more reliable way than conventional others: 1) to observe the negative spike in the electron current of the sample by biasing a positive voltage; 2) to observe the

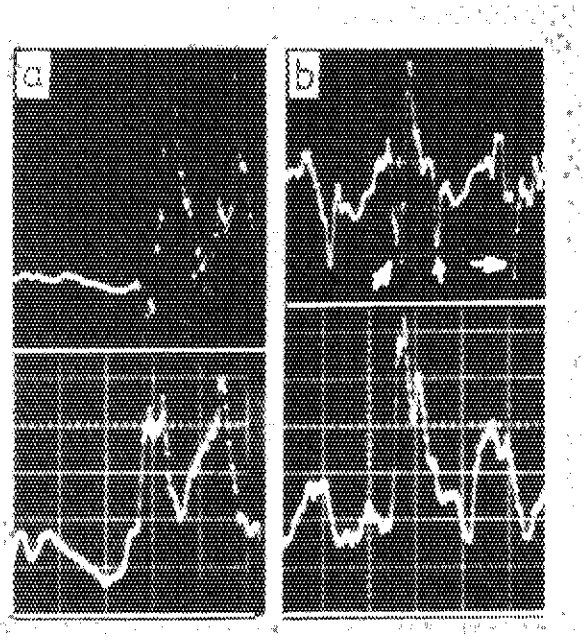

Fig. 7 Oscillogram traces of sample current in a) ion (5 A/div.) and b) electron (20 A/div.) at the unstable phase of discharges (50 μs /div.). Arrows indicate negative spikes in the electron current. Langmuir probe signals obtained simultaneously are shown below. Base lines are shown by white lines.

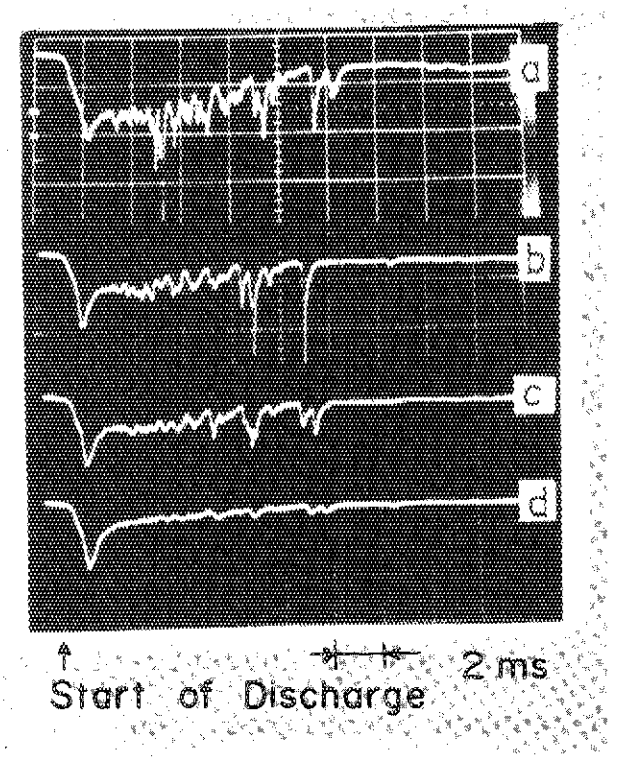

Fig. 8 Light signals (upside down) from a sample for a) the first exposure, b) the second, c) the third, d) the background (the sample was pulled out). 2 ms/div.

conditioning effect in the pulsive signals. It should be noted that Fig. 8 is the first presentation that shows the conditioning effect observed by real time methods. From these measurements, recent understanding that arcing occurs at the spike is confirmed.

§5. Measurement of plasma parameters related to the arc initiation

In this section, let us focus our interest into the plasma at the spike phase. Figure 9 shows an oscillogram of hard X-ray, the sample current and the light emission from the sample obtained simultaneously during the initial unstable phase of a discharge. The figure shows that the hard X-ray emission coincides with the spike of the sample current and the light. This correlation has already been observed in our previous work [6] where we inferred that runaway electrons produce enough potential difference between the plasma and the material to initiate arcing. Plasma parameters related to arcing, however, have been unknown so far. A study of the dependence of arc initiation on plasma parameters is important because, for example, it may predict whether unipolar arcs will occur or not even during stable discharges in future tokamaks. We present here results of measurements of plasma parameters with respect to arc initiation in the scrape-off layer of the JFT-2 tokamak.

Figure 10 shows a variation of the peak hight of a spike in the probe signal (as shown in Fig.6) as a function of bias voltage that was changed shot by shot. Although there is some scatter in the data points, a good double probe characteristics is manifest, even at the spike. This result owes

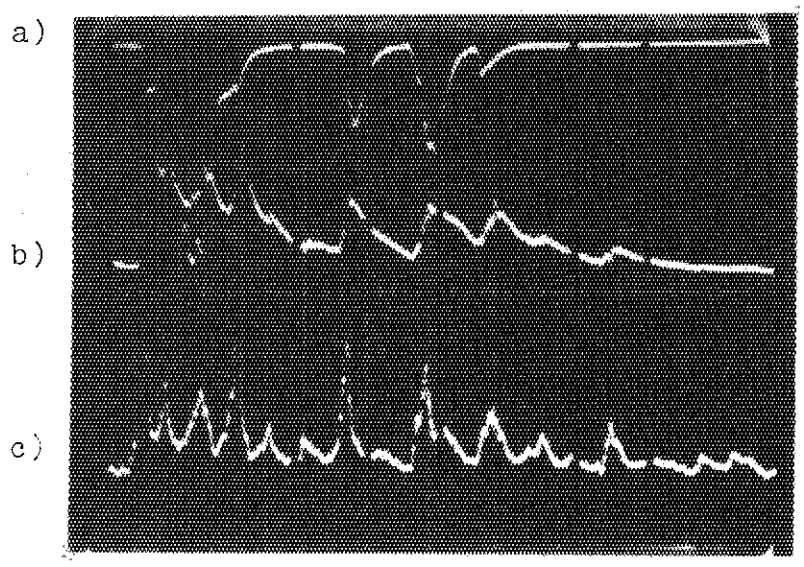

Fig. 9 Oscillogram traces of a) hard X-ray (up-side down), b) light emission from a sample, c) current through the sample obtained simultaneously during the unstable phase of a discharge. 200 μs/div.

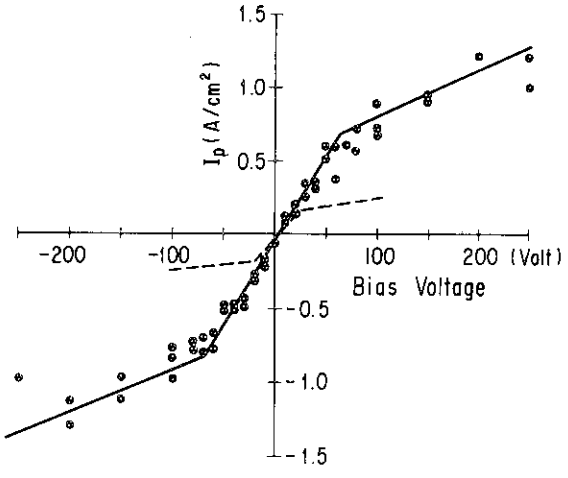

Fig. 10 Double probe characteristics at spike (solid line) and in stable phase (dotted line).

to the reproducibility of the discharge mentioned already. A typical probe characteristic in the stable phase is also shown in this figure. It was found from these measurements that the electron temperature T_e is about 30 to 60 eV at the peak of spikes and 10 to 20 eV during the subsequent stable discharge with electron density of $n_e = 2 \times 10^{12}$ cm^{-3} and 6×10^{11} cm^{-3}, respectively. Note that these absolute values vary with the plasma condition and the probe position. So, we shall focus our interest on the relative values.

The floating potential ϕ_f in the limiter shadow during the initial phase of a discharge is shown in Fig. 11a. It is found that values of ϕ_f lie above +500V at the spikes and +50V during the rest of the discharge. The space potential ϕ_s, which corresponds to the potential difference between the plasma and the wall, can be estimated from $\phi_s = \phi_f + 4T_e/e$ where e is the electronic charge [9]. Hence, ϕ_s is above 700V at the spike and 100V elsewhere.

Figure 11b shows the floating potential inside the radius of the aperture limiter (compare Fig. 11a). In this measurement, to catch runaway electrons effectively, we used a sample similar to that of Fig. 4 as a probe. The polarity of the spikes was altered. The conclusion drawn in the previous work with the measurement of hard X-ray emission - that runaway electrons produce a large potential gap - is supported by these figures, i.e. when the probe was located inside the limiter, runaway electrons first impinged on the probe. Hence, ϕ_f of the spikes was detected to be negative. On the other hand, in the limiter shadow, the runaway electrons were stopped by the limiter, so the probe detected the remaining

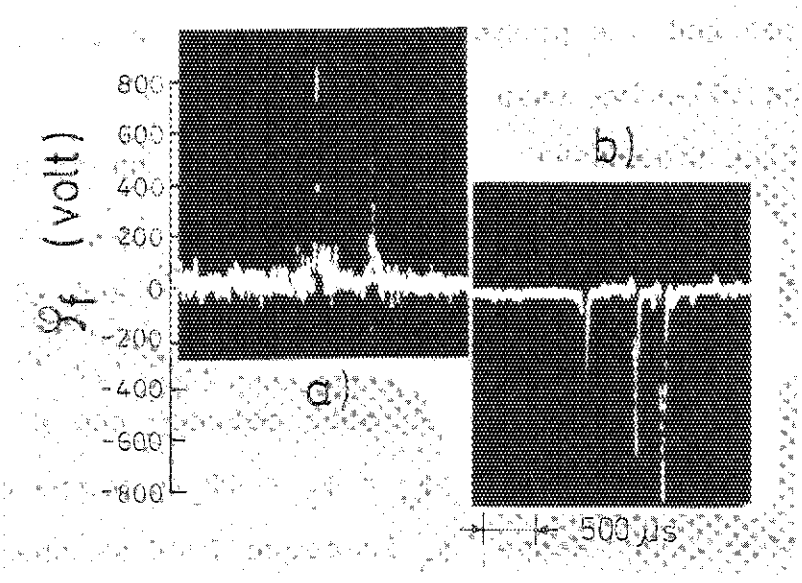

Fig. 11 Floating potential ϕ_f ; a) 1 cm outside, b) 1 cm inside aperture limiter radius during unstable phase.

positive plasma.

To this end, let us discuss the dominant cause of the arc initiation. The strength of the electric field perpendicular to the cathode surface is one of the important parameters in arc initiation. For unipolar arcing, this role is played by the potential difference across the sheath region. On the assumption that the entire electric field is concentrated within the sheath, the sheath electric field E_s can be estimated from

$$E_s = \frac{4T_e/e + \phi_f}{\lambda_D}$$

where λ_D is the Debye shielding length. The change in λ_D is small even at the spike because the rate of increase in the temperature coincides with that in the density. Since ϕ_f is larger than $4T_e/e$, we may conclude that the pulsed runaway electrons play the dominant role in arc initiation. The contribution of the enhanced T_e and n_e are, however, non-negligible. In particular, they may supply enough current to sustain arcing to electrically isolated components.

§6. Asymmetry of arc tracks and plasma behavior

As is pointed out in §3, an asymmetry of arc tracks left on limiter surfaces has been generally found in tokamak devices [10,11]. However, any proper explanation to the cause of the phenomena has not been presented yet. We should like to explain the mechanism here with a measurement of ion motion in the tokamak magnetic field.

Figure 12 shows radial profiles of the ion saturation current obtained by using a directional probe in the median plane of the scrape-off-layer: a) at a stable phase and b) at a spike. The ion flux to the ion side is much larger than that to the electron side. This difference is due to ion drift orbits in the poloidal magnetic field: namely, based on a similar mechanism to the ion diamagnetic current at the density gradient [12]. In our case, the banana width, defined by $2\Delta r = 2q\rho(R/r)^{\frac{1}{2}}$ [13], is 9 mm where $q = 4$ is the safety factor; $\rho = 0.6$ mm is the ion Larmor radius (assuming that $T_i = 30$ eV for $B_t = 1.3$T); $R = 90$ cm is the plasma position; $r = 27$ cm is the radial position of the measurement from the center of the plasma. This agrees with about 10 mm separation between the ion and electron side profiles in Fig. 12a. Because of a large scatter in the data, a quantitative consideration may be somewhat difficult in the spike case, but the asymmetry is clearly shown.

We consider the difference of the ion fluxes in the toroidal direction is the cause of the asymmetry of the arc frequencies. Possible explanations might be as follows; (1) since larger ion flux corresponds to higher plasma density near the material surface, the sheath electric field is enhaced on the ion side in such a way as to increase the possibility of arcing; or, (2) ion impacts directly trigger the arc initiation, for example, by the enhancement of secondary electron emission. There is no chance for runaway electrons to directly trigger the ignition because they hit the electron side of the sample. However, the role of the large potential difference produced by runaway electrons does not alter these explanations. Since both plasma and wall

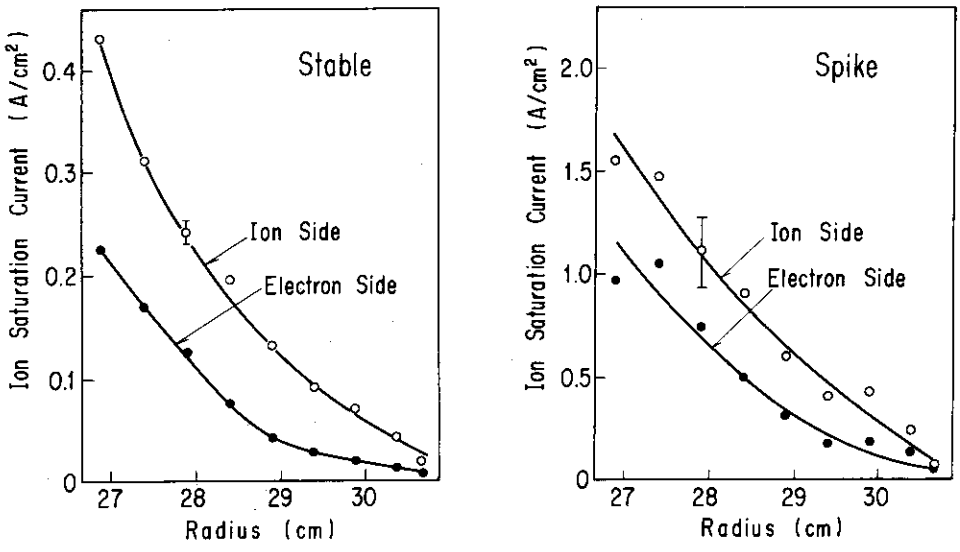

Fig. 12 Radial profiles of ion saturation current obtained by directional probe in median plane; a) during stable phase, b) at spike.

are conductors, this potential difference is distributed all over the plasma-wall interface. In these circumstances, the inhomogeneity of the ion flux density determines the place where preferential initiation of arcing occurs.

§7. Discussion and Conclusions

The results that we have obtained from the present study are:

(1) More reliable detection techniques than others were added to the real time observation method of arcing;

(2) Measurements of plasma parameters made it possible to clarify the dominant cause of the arc initiation on the tokamak first wall;

(3) It was found that ion drift motions in the boundary region is related to some aspects of the plasma-wall interaction.

We can conclude the cause of unipolar arcs on the tokamak first wall as follows. In the current rising phase of a plasma discharge, runaway electrons are produced due to low plasma density and high loop voltage. Since the plasma is very unstable in this period, runaway electrons instantaneously escape to the wall because of disruptions. The ambipolar condition breaks down and electric potential between the plasma and the wall increases. The high energy of runaway electrons makes the potential large enough to initiate unipolar arcing. Moreover, T_e and n_e enhanced by the plasma onset increase the electric field strength in the sheath region. That also contributes to the arc initiation, especially on ion side, and sustains the arc current. The reason why it is hard to develop unipolar arcs during the stable

phase of a discharge is, therefore, clarified.

The ion drift motion in a tokamak boundary plasma was first detected, by using a directional probe, in the JFT-2a experiment as described in Chapter 3. The present experiment showed that the ion drift motion affects arcing on the first wall. The asymmetry of the impurity fluxes onto an impurity probe as observed in several tokamak [14,15,16] can also be interpreted in terms of a drift motion. The ion drift motion in the boundary region seems to be important for the plasma-wall interaction in a tokamak device.

On the basis of the present measurements, let us here discuss the problem of a limiter in contact with a high-temperature and high-density plasma in a future tokamak. A potential difference of 800 V at a spike is equivalent to a plasma temperature of about 200 eV, normal sheath condition being assumed. With this temperature of about 200 eV and density of 2×10^{12} cm^{-3}, the calculation of the heat flux density from $Q = \gamma I_s T_e$ [17], where γ is the conversion coefficient between particle and heat fluxes (usually $\gamma = 8$), results in $Q = 4.6$ kW/cm^2. Such a high heat flux density is intolerable for any meterial. On the other hand, in the present experiment we found that plasma exposure exerts an appreciable conditioning effect on a sample surface. Shot-by-shot reduction of arcing was observed by the real time observation method. In an experiment carried out at ISX-B [18], a similar strong conditioning effect has been observed. These results predict that on a well conditioned surface arcing will hardly occure in spite of large electric

fields. The boundary plasma should, therefore, be controlled because of the thermal problem.

PART II: THE CAUSE OF THE MOTION OF ARCS IN THE PRESENCE OF A MAGNETIC FIELD

§1. Introduction

From the first observation of a peculiar motion of arcs in a magnetic field, the phenomenon has attracted a strong interest of scientists. Many theories to explain the mechanism of the motion have been proposed so far. Shortly speaking, these theories seem to be insufficient to explain fully the behavior of the motion. The basic ideas of these theories can be classified into two large groups: magnetohydrodynamic (MHD) approach and kinetic approach (to condider motions of charged particles). The former is made by being put an emphasis on specific MHD forces which move the arc column. On the other hand, the latter is based on the individual or collective charged particle motion. We should like to leave the criticizm on each theory to some other review articles[19].

Characteristic features of the phenomena are;

(a) the motion becomes retrograde with a decreasing gas pressure lower than some critical value which depends on the magnetic field and the arc current[20];

(b) the velocity of the motion increases with increasing the magnetic field[21-24];

(c) when the magnetic field is inclined to the plane of the cathode, the direction of the motion is no longer transversal, but has a component in the direction of the magnetic

field[25,26] (see Fig. 13).

Any mechanism proposed as a cause of the motion should account for above mentioned behavior. In this part, as a possible mechanism, we propose a theory on the basis of the kinetic approach.

§2. Theory

An important point of the theory based on the kinetic approach is that it takes a mechanism of the arc initiation into the consideration. The motion of arcs is attributed not to some forces but to a change of the arc spot by an excitation of a new spot in the characteristic direction of the old spot. The succession of the change results in a movement of the arc column. The initiation of arcing is closely related to the secondary electron emission from the surface. It is considered that the secondary electron emission is caused by impacts of charged particles. Therefore, we concentrate our interests on the analysis of the motion of charged particles near the arc column.

Here, we consider ions which are desorbed or evaporated at an arc spot and ionized in the arc column. The ion receives kinetic energy and flies out of the arc column. The motion of ions in the plane perpendicular to the magnetic field is shown schematically in Fig. 14. Ions moving in the parallel direction are less important in the present discussion. Owing to the gyromotion, a particular region of the material surface, which lies in the retrograde direction from the arc spot, suffers more ion impacts than others as seen in the figure. The direction of

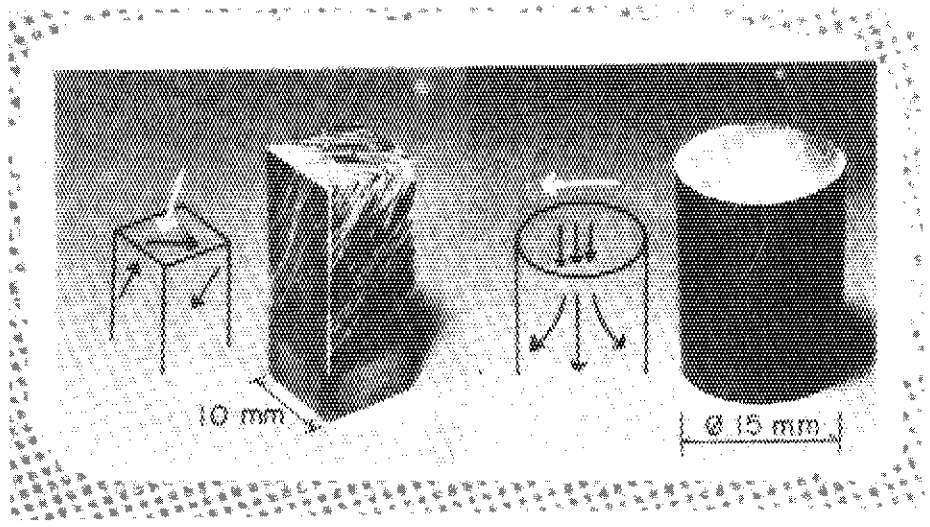

Fig. 13 Arc tracks of oblique motion on both plane and curved surfaces. The white arrows indicate direction of the magnetic field parallel to the top surface and the black arrows illustrate direction of the motion.

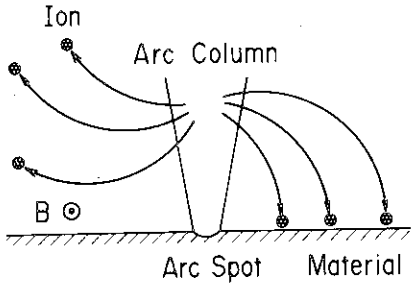

Fig. 14 Motion of ions produced in the arc column in the plane perpendicular to the magnetic field. The right-hand side of the arc column is the retrograde side.

the motion is determined by such an asymmetry of the ion flux density onto the surface. In the following, we have the ion flux density as a function of the distance from the arc spot.

To begin with, we introduce a co-ordinate system xyz putting the arc column on the z axis, the material surface on the xy plane and the magnetic field normal to the xz plane. For the simplisity, the following conditions are assumed: 1) most ionizations occur in a narrow region of the column; 2) the ions get the same energy at the ionization; 3) the ions are ejected uniformly in all directions. A typical ion motion is shown in Fig. 15: the ionization occurs at P and the ion motion is stopped at Q.

The flux density I at Q is given by

$$I = \frac{g}{4\pi S} \frac{d\theta}{dx} \tag{1}$$

where g is the ion production rate at P, θ is the angle of ejection in the xz plane and S is the length of the orbit PQ. After simple calculations, $d\theta/dx$ and S can be expressed by

$$\frac{d\theta}{dx} = \frac{x - \rho\sin\theta}{\rho(x\cos\theta - \ell\sin\theta)} \tag{2}$$

and

$$S = 2\rho\sin^{-1}\left(\frac{\sqrt{\ell^2 + x^2}}{2\rho}\right) \tag{3}$$

where ρ is the ion gyroradius and ℓ is the length of OP (the ionization length). Figure 16 shows $(1/S)(d\theta/dx)$ as a function of x with the parameter dependence on ρ. In this figure, the retrograde side corresponds to the positive x side. The most noticeable feature of the figure is that the calculated flux

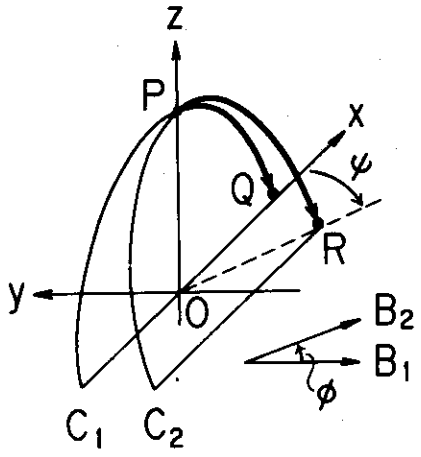

Fig. 15 Typical orbit of an ion. Semi-circles C_1 and C_2 represent orbits when the magnetic field is normal to the xz plane (B_1) and is inclined in the yz plane (B_2), respectively. Ions are produced at P and hit the material surface at Q or R.

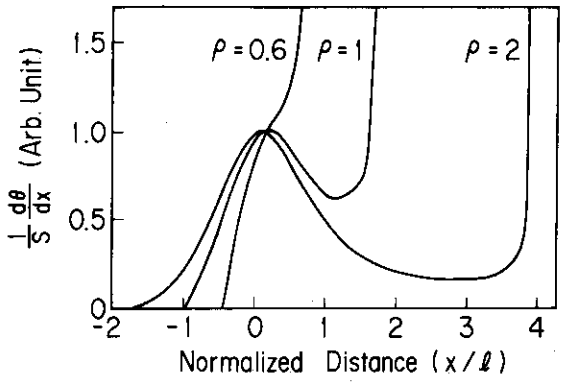

Fig. 16 Relative strength of the ion flux density along the x axis with the parameter dependence on the ion gyroradius ρ. Both the distance from the arc spot and the gyroradius are normalized by the ionization length ℓ.

density becomes infinite at the particular point of x: $x_c = (4\rho^2 - \ell^2)^{\frac{1}{2}}$. This intence ion flux gives the most strong probability of succeeding arcing to the spot. We consider this focussing of ion orbits is the key mechanism of the retrograde motion. The similar focussing is well known in the ion beam optics of ion sources[27].

§3. Interpretation of typical behavior

In the following, let us examine the validity of the theory by explaining the typical characteristics of the motion mentioned earlier.

(a) Pressure dependence. As has been commonly considered, collisions disturb the ion gyromotion. Hence, in a high pressure discharge, retrograde motion is rarely observed.

(b) Dependence of the velocity on the magnetic field. The velocity of the motion V_R can be written as

$$V_R = \frac{x_c}{t_D} = \frac{\sqrt{4\rho^2 - \ell^2}}{t_D} \qquad (4)$$

where t_D is the time required for the development of a new arc spot. To evaluate the absolute value of t_D is difficult within our present knowledge. However, we may say that a greater ion flux density causes more rapid development of arcing. Hence, we assume, putting k as a constant,

$$t_D = \frac{k}{I} \quad . \qquad (5)$$

Since $d\theta/dx$ at x_c is infinite, we estimate the relative strength of I at the point Δx apart from x_c. At that point $d\theta/dx$ can be

expressed by

$$\frac{d\theta}{dx} = \frac{-1}{\Delta\theta}\left(\frac{d^2x}{d\theta^2}\right)^{-1} \tag{6}$$

where $\Delta\theta$ is a small increment of θ corresponding to Δx. At x_c we have

$$\frac{d^2x}{d\theta^2} = -\frac{4\rho^2}{\sqrt{4\rho^2 - 1}} \tag{7}$$

and

$$S = \pi\rho \tag{8}$$

where, for the simplisity, we put $\ell = 1$. Combining these relation (1) and (4)-(8), we have

$$V_R \propto \frac{4\rho^2 - 1}{4\rho^3} \tag{9}$$

or

$$V_R \propto 4B - B^3 \tag{10}$$

where B is the normalized magnetic field defined by $B = \ell/\rho$.

Relation (10) gives us a simple picture. That is, in the region of weak B, V_R increases in proportion to B, then reaches a saturation level and decreases towards zero with a further increase of B. Up to the saturation, this behavior agrees with all observations[21-24]. St. John and Winans[22], however, did not observe this decreasing behavior. Moreover, they have found a further jump of the velocity with an increase of B. This discrepancy, however, does not show the inconsistency of the present theory. They observed a change in the plasma condition with the increase of B. Our theory assumes that the plasma conditions are constant. On the other hand, Sethuraman and Barrault[24] have reported that retrograde motion towards

the higher magnetic field region ceased at a critical value of the magnetic field. It is possible to explain their observation by this theory.

(c) Oblique motion in the magnetic field of an oblique angle of incidence. This specific motion can be explained by using also the illustration of Fig. 15. If the magnetic field is inclined in the yz plane as B_2, the gyromotion perpendicular to the magnetic field changes from C_1 to C_2. It should be noted that focussing of the ion orbits appears only on the plane perpendicular to the magnetic field. Hence, the focussing point shifts on the material surface with the inclination as is shown in Fig. 15. If R is the focussing point, the resulting arc motion is found in the direction of OR, having a drift component in the y direction. The drift angle ψ as a function of the field inclination ϕ can be expressed by

$$\psi = \sin^{-1}\left(\frac{\ell\tan\phi}{\sqrt{4\rho^2 - \ell^2}}\right) \quad . \tag{11}$$

Robson[26] has obtained experimentally a relation between ϕ and ψ in which the drift angle increases with the angle of inclination and with the magnetic field. Qualitative features of relation (11) agree with Robson's observation. A similar argument can be made for a curved surface: that is, resulting tracks are curved as have been observed by McCracken and Goodall[3]. As the angle of the surface approaches perpendicular to the magnetic field, the ion flux for the new arc spot decreases or the ion orbit no longer intersects the xy plane, and arcs diminish consequently.

Typical aspects of the retrograde motion can, thus, be clearly explained. Therefore, we should like to propose the

mechanism as the most probable cause. In addition to these facts, it can be found in Fig. 13 that a moving arc can turn a corner and continue its motion on the neighboring surface. This behavior can easily be explained by the mechanism described here.

§4. Discussion

The present analysis has been made on the basis of a simplified model which neglects the distribution of the kinetic energy of ions, the spread of the ionization region and an effect of the electrostatic force. However, we may say that the basic role of the gyromotion is not altered by the inclusion of these effects. A quantitative analysis is not possible at this stage due to insufficient knowledge concerning the arc column (plasma)-related phenomena. In particular, for this theory it is necessary that the ionization length agrees with the ion gyroradius in order of magnitude. Unfortunately, reliable data to verify this condition have not appeared in the literature as yet.

To this end, we should like to discuss the control of the motion. The fact that the motion diminishes on a curved surface at some critical angle to the magnetic field suggests a possibility of control of the motion by means of a geometrical consideration. It has been pointed out, however, that the retrograde motion is much influenced by the surface condition [20,23,24,28]. Also a considerable conditioning effect has been observed in studies of unipolar arcs at the tokamak first wall as described in the former part of this chapter. Therefore, it may be practical to employ relevant conditioning

processes rather than the geometrical one to control the plasma contamination from the retrograde motion.

In conclusion, a possible mechanism which is consistent with several observations of the retrograde motion is presented.

REFERENCES

[1] A.E. Robson and P.C. Thonemann, Proc. Phys. Soc. 73 (1959) 508.

[2] J.L. Craston et al., in Peaceful Uses of Atomic Energy (Proc. 2nd Int. Conf. Geneva, 1958) Vol.32, UN, Geneva (1958) P 414.

[3] G.M. McCracken and D.H.J. Goodall, Nucl. Fusion 18 (1978) 537.

[4] J. Stark, J. Phys. Zeitschrift, 4 (1903) 440.

[5] K. Ohasa et al., Nucl. Fusion 18 (1978) 872.

[6] M. Maeno et al., Nucl. Fusion 20 (1980) 1415.

[7] D.H.J. Goodall and G.M. McCracken, Nucl. Fusion 19 (1979) 1396.

[8] P. Mioduszewski, R.E. Clausing and L. Heatherly, J. Nucl. Mater. 85 & 86 (1979) 963.

[9] F.F. Chen, Plasma Diagnostic Techniques (R.H. Huddelstone and S.L. Leonard Eds) Chap.4, Academic Press, New York (1965) P 178.

[10] D. Hildebrandt et al., J. Nucl. Mater. 93 & 94 (1980) 310.

[11] R.A. Langley et al., J. Nucl. Mater. 93 & 94 (1980) 479.

[12] L. Spitzer Jr., Physics of Fully Ionized Gases, Interscience Publishers, 1962, Chap.2, P 32.

[13] H.P. Furth, Nucl. Fusion 15 (1975) 478.

[14] G. Staudenmaier, P. Staib and W. Poschenrieder, J. Nucl. Mater. 93 & 94 (1980) 121.

[15] V.M. Chicherov et al., J. Nucl. Mater. 93 & 94 (1980) 133.

[16] P. Staib, H.F. Dylla and S.M. Fossnagel, J. Nucl. Mater. 93 & 94 (1980) 166.

[17] G.D. Hobbs and J.A. Wesson, Plasma Phys. 9 (1967) 85.

[18] R.E. Clausing, L.C. Emerson and L. Heatherly, J. Nucl. Mater. 93 & 94 (1980) 150.

[19] V.I. Rakhovskii, IEEE Trans. Plasma Sci., PS-4 (1976) 81.

[20] C.J. Gallagher and J.D. Cobine, Phys. Rev. 71 (1947) 481.

[21] C.G. Smith, Phys. Rev. 62 (1942) 48.

[22] R.M.St. John and J.G. Winans, Phys. Rev. 94 (1954) 1097.

[23] J.C. Sherman et al., J. Phys. D: Appl. Phys. 8 (1975) 696.

[24] S.K. Sethuraman and M.R. Barrault, J. Nucl. Mater. 93 & 94 (1980) 791.

[25] C.G. Smith, Phys. Rev. 69 (1946) 96.

[26] A.E. Robson, Proc. Int. Conf. on Phenomena in Ionized Gas, Uppsala, 1959, Vol.1 (1960) P 346.

[27] G.F. Weston, Vacuum 30 (1980) 49.

[28] T.J. Lewis and P.E. Secker, J. Appl. Phys. 32 (1961) 54.

5 Impurity Buid-Up in Fusion Devices

§1. Introduction

Metal impurities in plasma which originate from the first wall have deleterious effects on plasma confinement as mentioned earlier. Sputtering, arcing and evaporation have been considered so far to be the dominant causes of the metal impurity introduction into plasma. The present study of arcing described in the previous chapter have brought an important conclusion that arcing scarcely occurs during the stable phase of plasma discharges. Evaporation can also be eliminated by a consideration to the thermal problem. Namely, the heat load of the first wall can be estimated from the output power and the area which receives the power. By a proper design of the device, we can avoid evaporation of material during normal plasma discharges. Sputtering, however, seems to be unavoidable at the tokamak first wall because the wall inevitably suffers impacts of particles from the plasma. Experiments made in JAERI tokamaks (JFT-2a and JFT-2) have exhibited that the metal impurity release during a stable discharge is caused mainly by sputtering[1,2]. Moreover, we found that oxygen ion is the dominant cause of sputtering. Figure 1 shows metal impurity (iron and titanium) levels in the JFT-2 plasma as a function of the oxygen content. The clear proportionality, especially in iron, shows that metals are introduced by sputtering by oxygen. The contribution of sputtering by working gas (hydrogen) looks negligibly small.

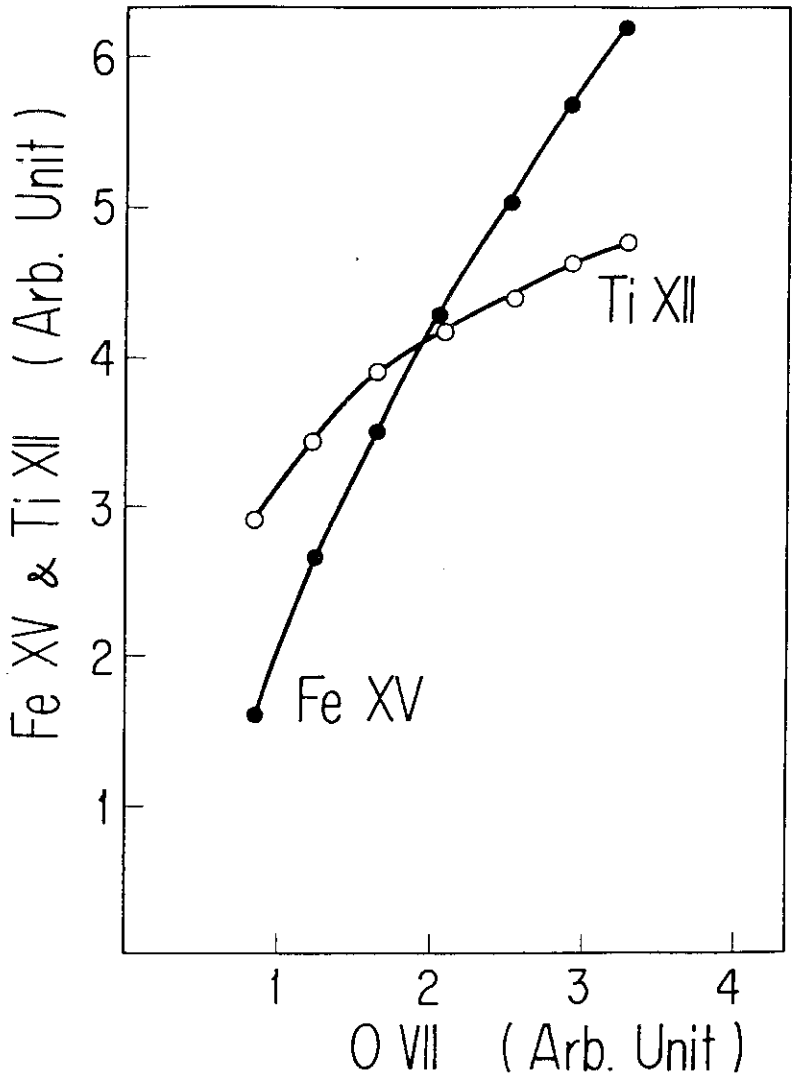

Fig. 1 Intensity of metal-impurity lines (Fe XV and Ti XII) as a function of oxygen line (oVII) intensity.

The difference of the behavior between iron and titanium in Fig. 1 can be understood by the well known fact that oxidized surface of titanium becomes resistant against sputtering.

In contrast with Fig. 1, an inverse proportionality is well known in several tokamak experiments[3-6]: the reduction of oxygen in the plasma caused an increase in the metal impurity concentration. What is the reason why such contradictory behavior appear in the tokamak plasma? In this chapter, we should like to deal with this problem. A self-consistent relation between light and metal impurities is derived in the following sections and its application to some plasma-wall interaction is examined.

§2. Theory

As mentioned earlier, the dominant cause of metal impurity release from the first wall is sputtering. In the following, we shall focus our interest on sputtering. In a steady-state discharge, the particle balance of the metal impurity in a plasma can be written as

$$\frac{N_M}{\tau_M} = S_G \frac{N_G}{\tau_G} + S_L \frac{N_L}{\tau_L} + S_M \frac{N_M}{\tau_M} \qquad (1)$$

where N, τ, S are the total number of particles, the particle confinement time, and the effective sputtering yield, respectively; the subscripts G, L, M refer to working gas, light impurity (primarily oxygen) and metal impurity, respectively. The contribution to sputtering from charge-exchange neutrals is negligible

in Ohmically-heated plasma[7]. 'Effective' sputtering yield means here that, among the sputtered particles, we only take those ions into account that enter the plasma main column. In other words, the shielding effect is included in this coefficient. As from here, we shall use the following notation:

T_e^b is the electron temperature of the boundary plasma,

n_e is the electron density,

P_{in} is the input power,

P_R is the radiation loss power,

γ is the conversion coefficient between particle and heat fluxes,

α is the rate coefficient for radiation loss power per impurity atom. The subscripts are the same as those mentioned above.

The key procedure of this treatment is the inclusion of some feedback effect in sputtering for the model to be self-consistent. First, we assume that the effective sputtering yield S is proportional to T_e^b, introducing an artificial coefficient σ:

$$S = \sigma T_e^b \quad . \tag{2}$$

For simplicity, we also assume $\tau = \tau_M = \tau_L = \tau_G$. Then, Eq.(1) becomes

$$N_M = (\sigma_G N_G + \sigma_L N_L + \sigma_M N_M) T_e^b \quad . \tag{3}$$

The boundary electron temperature can be determined by the convective/conductive power loss and the particle flux to the first wall[8]:

$$T_e^b = \frac{P_{in} - P_R}{e\gamma \frac{N_G}{\tau}} \tag{4}$$

where $e = 1.6 \times 10^{-19}$.

If the energy loss by charge-exchange neutrals is non-negligible, the input power P_{in} in Eq.(4) has to be adjusted by this amount. In a zero-dimensional model, the radiation loss power can be expressed by

$$P_R = \alpha_L n_e N_L + \alpha_M n_e N_M \quad . \tag{5}$$

In this expression, all the radiative phenomena are averaged and assumed to be proportional to the number of impurity atoms. We neglect the radiation loss due to hydrogen and the ionization energy loss. Combining Eqs.(3), (4) and (5), we obtain

$$N_M = (\sigma_G N_G + \sigma_L N_L + \sigma_M N_M) \frac{P_{in} - (\alpha_L n_e N_L + \alpha_M n_e N_M)}{k N_G} \tag{6}$$

where $k = e\gamma/\tau$.

The solution of Eq.(6) for the metal impurity concentration is

$$\frac{N_M}{N_G} = A - \frac{\sigma_L N_L}{\sigma_M N_G} + \left\{ A^2 + \frac{k}{\alpha_M \sigma_M n_e} \left(\frac{\sigma_L N_L}{\sigma_M N_G} + \frac{\sigma_G P_{in}}{k N_G} \right) + \left(\frac{\sigma_L}{\sigma_M} - \frac{\alpha_L}{\alpha_M} \right) \frac{\sigma_G N_L}{\sigma_M N_G} \right\}^{\frac{1}{2}} \tag{7}$$

where $A = \frac{1}{2} \left(\frac{\sigma_L}{\sigma_M} - \frac{\alpha_L}{\alpha_M} \right) \frac{N_L}{N_G} + \frac{\sigma_M P_{in} - k N_G}{2\alpha_M \sigma_M n_e N_G} - \frac{\sigma_G}{2\sigma_M}$.

This is a self-consistent relation between light and metal impurities.

§3. Application to actual situations

In the following, we shall examine whether the relation is consistent with an actual tokamak plasma or not. Fortunately, the TFR experiment has reported data[9] which seem to be suitable for the application of Eq.(7). Data of this kind are rarely to be found in the literature so far. In Table 1 of Ref.[9] eight different cases of plasma discharges with many plasma parameters are shown. These parameters enable us to evaluate N_G, N_L, N_M, n_e and P_{in}. Measurements of γ and τ are also described in the text; $\gamma = 15$ and $\tau = 10$ ms have been determined. Hence, for the use of Eq.(7) it is necessary to evaluate α_L, α_M, σ_G, σ_L and σ_M here. A simple way of evaluating quantities is optimizing them with the experimental results in order to satisfy Eqs.(3) and (5). By using the least-squares method, the coefficients can be determined as follows: $\alpha_L = 7.4 \times 10^{-27}$ (W-cm^3); $\alpha_M = 5.0 \times 10^{-26}$ (W-cm^3); $\sigma_G = 3.1 \times 10^{-7}$ (eV)$^{-1}$; $\sigma_L = 1.2 \times 10^{-3}$ (eV)$^{-1}$ and $\sigma_M = 1.0 \times 10^{-2}$ (eV)$^{-1}$. Substituting these values into the equation, we can obtain calculated metal impurity concentration as shown in case a) of Table 1. A comparison with the experimental result shows rather a small discrepancy between experimental and calculated results (within a factor of 2, except for one case) while the ratio N_L/N_G varies by an order of magnitude. We should like to note that the values of α_L and α_M agree, in order of magnitude, with a calculation of the impurity radiation by Jensen and others[10]. On the other hand, the physical foundation of the values for σ seem to be unclear. The small value of σ_G suggests that sputtering by the working gas is negligible.

Table 1 The metal impurity concentration in TFR: calculated and experimental results as a function of several plasma parameters

Quantity			TFR Case in Ref.[9]							
			1	2	3	4	5	6	7	8
N_M/N_G	Calculated	(10^{-4}) a)	3.7	2.3	1.2	2.0	1.3	3.1	1.3	4.2
		b)	2.9	2.0	2.8	3.1	2.0	3.7	2.0	4.3
	Experimental	(10^{-4})	3.6	5.4	0.83	2.14	2.0	5.3	1.25	4.0
Related parameters	N_L/N_G	(10^{-4})	220	170	17	29	40	53	40	53
	P_{in}	(kW)	500	520	405	530	410	630	410	740
	n_e	($10^{13}cm^{-3}$)	5.5	6.5	6.0	7.0	7.5	7.5	7.5	7.5

JAERI - M 84 - 195

To see whether the above evaluation is reliable, another evaluation of σ was made, based on sputtering data from laboratory experiments[11-13]. The evaluation procedure is similar to that of Ref.[7], with an assumption that T_e^b = 30 eV. The shielding efficiency was adjusted so as to fit the calculation to the experimental results. As a result, we obtained $\sigma_G = 6.7 \times 10^{-6}$ $(eV)^{-1}$, $\sigma_M = 6.7 \times 10^{-4}$ $(eV)^{-1}$ and $\sigma_M = 1.3 \times 10^{-3}$ $(eV)^{-1}$. This corresponds to a situation where sputtering by the working gas is dominant. Using these values of σ, another result of the calculation is obtained as case b) in Table 1. A comparison shows that the calculation using the former σ approximates the impurity behavior better than the latter σ. Any change in σ_G of the latter case does not improve the situation. The result suggests that the metal impurity release is mainly caused by impurity sputtering. A possible explanation for such a low sputtering yield by the working gas is as follows: The boundary plasma temperature may be lower than we have expected. Hence, the D^+ ions only receive energy of about the sputteing threshold. This results in a marginal contribution of deuterium sputtering.

Let us next examine a parameter dependence of the metal impurity concentration in accordance with the model equation. First, we assemble model parameters as shown in Table 2, which are taken from the evaluation described abvoe. Figure 2 shows the variation of the metal impurity concentration N_M/N_G as a function of the light impurity concentration N_L/N_G when the other parameters in Eq.(7) are fixed. Case A in the figure was calculated by using the parameters of Table 2. Case B and C

Table 2 Model parameters for the use of Eq. (7)

parameter	Value
P_{in}	500 (kW)
τ	10 (ms)
γ	15
α_L	7.4×10^{-27} $(W\text{-}cm^3)$
α_M	5.0×10^{-26} $(W\text{-}cm^3)$
σ_L	1.2×10^{-3} $(eV)^{-1}$
σ_M	1.0×10^{-2} $(ev)^{-1}$
σ_G	3.1×10^{-7} $(eV)^{-1}$
N_G	5.0×10^{19}
n_e	7.0×10^{13} (cm^{-3})
N_L/N_G	3.0×10^{-3}
N_M/N_G	1.8×10^{-4}

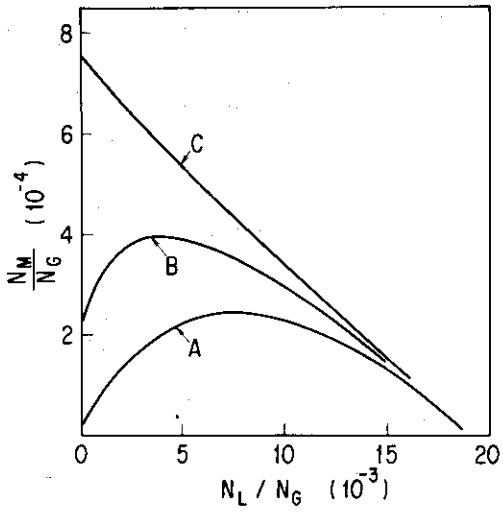

Fig. 2 Variation of metal impurity concentration N_M/N_G as function of light impurity concentration N_L/N_G: Case A is calculated by substituing parameters of Table 2; cases B and C are obtained by increasing σ_M 2.5 and 3.3 times the value of case A, respectively.

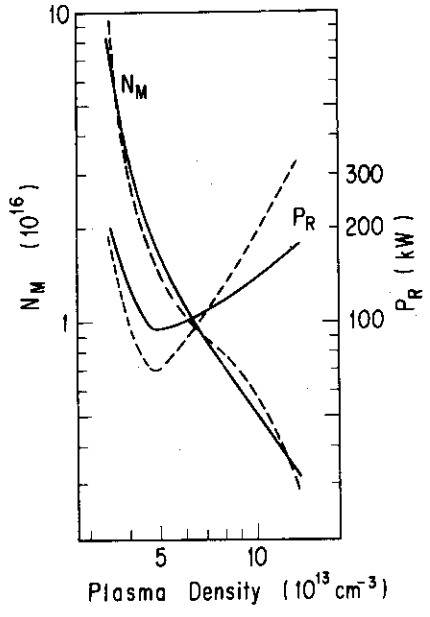

Fig. 3 Variation of metal impurity as function of plasma density. Radiation power loss P_R is also shown. Solid and dotted lines designate constant-N_L and constant-N_L/N_G cases, respectively.

were obtained by changing the coefficient σ_M 2.5 times and 3.3 times, respectively, the value of case A. We see that the relationship between metal and light impurities in a plasma is largely characterized by the self-sputtering yield if σ_G is small enough. Since the self-sputtering yield depends on the boundary temperature, a similar result can be obtained by varying input power or the parameter γ/τ (see Eq.(4)). The ambivalent role of the light impurity in the introduction of the metal impurity that was mentioned earlier can be understood by a figure of this kind.

Case A shows that if the sputtering yields is sufficiently small the metal impurity concentration becomes nearly zero when the light impurity concentration decreases. A divertor reduces the effective sputtering yield by a sufficient shielding efficiency[14], so that it is interesting to note that two methods for reducing the metal impurity in a plasma - edge cooling by the light impurity injection[15] and the divertor - correspond to the right- and left-hand sides of case A, respectively. On the contrary, in cases B and C with large sputtering yields, the metal impurity level at $N_L = 0$ is maintained on some finite level by self-sputtering only. Because of the steady state, the effective sputtering yield is just unity there. In other words, the metal impurity build-up in a plasma is automatically limited to a certain level, owing to radiation self-cooling.

Relation (7) can be used to exhibit another aspect of the plasma-wall interaction as shown in Fig. 3 where the dependence of the total amount of metal impurity N_M on the plasma density is given. The corresponding radiation power loss P_R is also shown.

The parameters in Table 2 are also used in the calculation. The solid lines indicate a case where the number of light impurities N_L is constant, while the dotted lines indicate a constant ratio N_L/N_G. The latter situation may represent a case where the light impurity is introduced by ion- or charge-exchange-neutral-induced desorption, while the former case simulates a constant influx of the light impurity due to outgassing or a vacuum leak. In both cases, a powerful reduction of the metal impurity with increasing plasma density (nearly n^{-2} dependence) is exhibited, whereas the radiation loss power does not vary that much. This effect may be one explanation for the reduction of the metal impurity by increasing the plasma density as has been shown in various tokamak experiments[2,16,17].

§4. Concluding remarks

We shall now discuss the validity of the approximation. One of the problems is the assumption of Eq.(2). In general, sputtering yields as a function of the incident energy show a threshold on the low-energy side and a peak at an appropriate energy. Since T_e^b is relatively low in the present situation, it may be aceptable to approximate S by a linear function of energy. An experimental result which supports this assumption has been presented in the PLT experiment, Fig. 6 in Ref.[6]. However, the assumption has no threshold in very-low-T_e^b region (corresponding to the right-hand side of Fig. 2). Hence, our result implies an overestimate there.

Another problem is the dependence of α on the plasma temperature. There was a concern that the present formulation

with constant α seems to be too simple to describe impurity behavior in tokamaks. The fact that Eq.(7) is a good approximation to the actual tokamak impurities suggests that the radiation loss power per impurity atom, in an average sense, is rather insensitive to the plasma conditions within the parameter range of Ohmically-heated plasmas.

To solve the problem in a more rigorous way, the analysis should be carried on by computer simulation since the problem is composed of many complicated phenomena: atomic and transport processes with multi-component, multi-dimensional and self-consistene modeling. This kind of treatment presented in this chapter may thus be the limit for an analytic solution of the problem.

Summarizing, we may say that an instructive relation helping us to understand some aspects of plasma-wall interaction has been presented in this study.

REFERENCES

[1] K. Ohasa et al., Nucl. Fusion 18 (1978) 872.

[2] N. Suzuki et al., in Controlled Fusion and Plasma Physics (Proc. 9th Europ. Conf. Oxford, 1979) Vol. 1, Culham Laboratory, Culham (1979) p90.

[3] E. Meservey et al., Suppression of Heavy Impurities in the ST Tokamak, PPPL Rep. MATT-1175 (1975).

[4] Equipe TFR, Nucl. Fusion 17 (1977) 1297.

[5] J. Hugill et al., in Controlled Fusion and Plasma Physics (Proc. 8th Europ. Conf. Prague, 1977) Vol. 1, Institute of Physics, Prague (1977) p39.

[6] K. Bol et al., in Plasma Physics and Controlled Nuclear Fusion Research (Proc. 7th Int. Conf. Innsbruck, 1978) Vol. 1, IAEA, Vienna (1979) p11.

[7] S. A. Cohen et al., J. Nucl. Mater. 76 & 77 (1978) 459.

[8] Y. Shimomura, Nucl. Fusion 17 (1977) 1377.

[9] TFR Group, J. Nucl. Mater. 93 & 94 (1980) 272.

[10] R. V. Jensen et al., Nucl. Fusion 17 (1977) 1187.

[11] J. Bohdansky, H. L. Bay and J. Roth, Proc. 7th Int. Vac. Congr. & 3rd Int. Conf. Solid Surface, Int. Union for Vac. Sci., Tech. and Applications, Vienna (1977) p1509.

[12] E. Hechtl, H. L. Bay and J. Bohdansky, J. Appl. Phys. 16 (1978) 147.

[13] H. L. Bay, J. Bohdansky and E. Hechtl, Rad. Effects 41 (1979) 77.

[14] S. Sengoku et al., Nucl. Fusion 19 (1979) 1329.

[15] Y. Shimomura, Nucl. Fusion 17 (1977) 626.

[16] B. Channici et al., in Controlled Fusion and Plasma Physics (Proc. 7th Europ. Conf. Lausanne, 1975) Vol. 2, Ecole Polytechnique Feferale, Lausanne (1975) p136.

[17] J. Fujita et al., in Plasma Physics and Controlled Nuclear Fusion Research (Proc. 7th Int. Conf. Innsbruck, 1978) Vol. 1, IAEA, Vienna (1979) p247.

6 SUMMARY

We found a cross-field plasma convection produced by an obstacle, in plasma confined in a toroidal multipole field. The mechanism of the formation of the convection could be explained by drift motions of plasma in magnetic field. The result brought us a general conclusion that inhomogeneity in a magnetically confined plasma causes a cross-field convection and resulting enhancement of anomalous plasma loss.

The experience in the multipole experiments has advanced in the study of tokamak boundary plasma in relation to divertor function and plasma-wall interaction. The divertor function and the boundary plasma behavior were successfully exhibited by the use of electrostatic method in the JFT-2a experiments. Also, a detailed study of arcing on the tokamak first wall was made by the measurement of the boundary plasma of JFT-2. Furthermore, a new theory which clarifies the cause of the motion of arcs in a magnetic field has been constructed on the basis of motion of a single particle.

The foregoing results about impurities helped us formulate a relation between light and metal impurities in a plasma. We showed that the relation well describes some fundamental aspects of the plasma-wall interaction.

We can find an interesting fact in this study that we could resolve some strange or unsolved plasma-related phenomena by a consideration of simple plasma motions in a magnetic field. We should like to claim here the importance of this point of view not only in the present study but also in future fusion researches.

AKNOWLEDGEMENTS

The author wishes to express his gratitude to Professor K.Kusukawa of Tokyo Metropolitan University for his encouragement and support during the preparation of this manuscript.

The author also would like to express his sincere gratitude to Professor K.Niu of Tokyo Institute of Technology whose continuous encouragement, support and advice have been invaluable.

It is a pleasure to thank colleagues of the plasma experiment groups of JAERI － JFT-1 group, JFT-2a group and JFT-2 group － for their valuable discussion and help. Particular thanks are due to Drs. S.Tamura, Y.Shimomura and N.Fujisawa for their continued supports during the experiments. The author is also deeply indebted to the operation group led by Mr. S.Kunieda for their reliable operation of the devices.

The continuing encouragement of Drs. S.Mori, Y.Obata, M.Tanaka, S.Tamura, Y.Tanaka and Y.Murakami of Fusion Research Center of JAERI is gratefully aknowledged.

REFERENCES THE THESIS ORIGINATED IN

Chap. 2

H.Ohtsuka et al : *Anomalous plasma loss in the JAERI toroidal hexapole,* JAERI-M 5469 (Report of Japan Atomic Energy Research Institute) (1974).

Chap. 3

H.Ohtsuka et al. : *Probe measurements in the scrape-off layer of a tokamak,* Plasma Phys. 20, 749-757 (1978).

Chap. 4

H.Ohtsuka et al. : *Unipolar arcs in JFT-2 tokamak,* J. Nucl. Mater. 93&94, 161-165 (1980).

H.Ohtsuka et al. : *Plasma parameters related to arc initiation on the tokamak first wall,* Nucl. Fusion 22, 823-826 (1982).

H.Ohtsuka : *A cause of the motion of arcs in the presence of a magnetic field,* Vacuum 33, 155-157 (1983).

Chap. 5

H.Ohtsuka : *A relation between light and metal impurities in tokamak plasmas,* Nucl. Fusion 22, 827-831 (1982).